United States Department of Agriculture

# Field Moisture Performance of Wood-Framed Walls with Exterior Insulation in a Cold Climate

**C.R. Boardman**
**Samuel V. Glass**
**Robert Munson**
**Borjen Yeh**
**Kingston Chow**

Forest Service | Forest Products Laboratory | Research Paper FPL–RP–698 | March 2019

## Abstract

Continuous exterior insulation is becoming more common in North America in above-grade exterior walls in both retrofit applications and new construction. It is used to improve the overall thermal performance of wall assemblies. The drying capability of wall assemblies with exterior insulation and an interior vapor retarder in cold climates is not well characterized. The moisture performance of wood-framed wall assemblies with and without exterior insulation was monitored during a 2-year period in the cold climate of Madison, Wisconsin, USA, under low and high interior humidity conditions and with intentional wetting of the wood structural panel sheathing. Moisture content and temperature of standard 38- by 140-mm wood framing and 11-mm-thick oriented strandboard (OSB) sheathing were measured in eight different wall assemblies, each with north and south orientation, in a conditioned test structure. Either a kraft paper or a polyethylene vapor retarder was used on the interior in combination with fiberglass cavity insulation. Exterior insulation was mineral wool, expanded polystyrene, or extruded polystyrene. The OSB sheathing was wetted in a controlled manner at three different times of year to investigate drying response. Wintertime moisture accumulation in OSB under the tested conditions was not a concern except in the wall with no exterior insulation and interior kraft vapor retarder, although rapid drying occurred in springtime. Exterior insulation had a predictable effect on wall cavity temperature. All 16 test walls were able to dry out quickly enough to keep moisture content below dangerous levels when challenged by modest water injection onto the interior OSB surface. The observed decrease in OSB moisture content after controlled wetting events was generally more rapid during warm weather than cold weather, more rapid with exterior insulation than without during cold weather, more rapid with vapor-open exterior insulation than vapor-tight exterior insulation during cold weather, and more rapid with interior kraft vapor retarder than with polyethylene.



Keywords: moisture performance, hygrothermal performance, durability, drying potential, exterior insulation, continuous insulation, building envelope, vapor retarder


## Contents




March 2019

Boardman, C.R.; Glass, Samuel V.; Munson, Robert; Yeh, Borjen; Chow, Kingston. 2019. Field moisture performance of wood-framed walls with exterior insulation in a cold climate. Research Paper FPL-RP-698. Madison, WI: U.S. Department of Agriculture, Forest Service, Forest Products Laboratory. 40 p.

A limited number of free copies of this publication are available to the public from the Forest Products Laboratory, One Gifford Pinchot Drive, Madison, WI 53726-2398. This publication is also available online at www.fpl.fs.fed.us. Laboratory publications are sent to hundreds of libraries in the United States and elsewhere.

The Forest Products Laboratory is maintained in cooperation with the University of Wisconsin.

# Field Moisture Performance of Wood-Framed Walls with Exterior Insulation in a Cold Climate

**C.R. Boardman,** General Engineer
**Samuel V. Glass,** Research Physical Scientist
**Robert Munson,** Engineering Technician
USDA Forest Service, Forest Products Laboratory, Madison, Wisconsin, USA

**Borjen Yeh,** Director, Technical Services Division
**Kingston Chow,** Building Scientist, Technical Services Division
APA – The Engineered Wood Association, Tacoma, Washington, USA

## 1 Introduction

The building envelope is a key component affecting overall building energy usage, and building codes have recently mandated higher insulation levels. Adding continuous exterior insulation has become a common strategy to improve overall thermal performance in North American above-grade exterior wall assemblies in both retrofit applications and new construction. This construction method is particularly relevant for wood-framed construction in cold climate zones. Although performance compliance paths in the International Energy Conservation Code (IECC) (ICC 2015) are often flexible in the design of exterior walls, the prescriptive compliance path requires wood-framed walls located in cold climate zones (IECC Climate Zone 6 or higher) to incorporate continuous insulation at a minimum level of 0.88 $m^2 \cdot K/W$ (5 $h \cdot ft^2 \cdot °F/Btu$) or R-5. This is often implemented with a split-insulated wall design that includes both cavity insulation and continuous exterior insulation (Fig. 1).

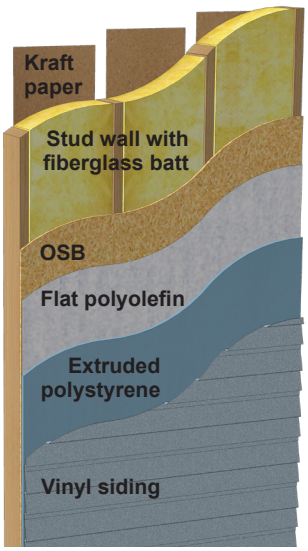


**Figure 1. Example of split-insulated wall with insulation both in the stud cavity and exterior of the sheathing system (OSB, oriented strandboard).**

Long-term moisture performance of exterior wall assemblies is a key consideration for contemporary energy-efficient structures. Improper design can lead to problems with moisture accumulation and subsequent degradation of materials. Although considerable research has been conducted on exterior insulation in wood-framed walls, further work is needed to provide a quantitative basis to minimize the risk from moisture performance and associated durability issues.

Moisture control strategies for exterior wall assemblies address the various sources of moisture interior and exterior of the building and the ways in which moisture migrates (TenWolde and Rose 1996). Exterior water management is critical to avoid bulk water intrusion. A continuous air barrier system minimizes moisture accumulation caused by uncontrolled air leakage. Vapor diffusion control strategies vary according to climate and properties of the materials in the assembly (Lstiburek 2004). In addition, wall assemblies should have the ability to dry out if they get wet (either during construction or during their service life). Drying potential is often a concern for wall assemblies that are insulated and air sealed to levels required by current model energy codes (Lstiburek 2013a, 2013b). Drying potential depends not only on the configuration of the wall assembly but also on the climate. Drying capability of wall assemblies with exterior insulation and an interior vapor retarder in cold climates is not well characterized.

Continuous exterior insulation raises the temperature of wood structural members in exterior walls during cold weather, relative to walls without exterior insulation, thereby decreasing the potential for wintertime moisture accumulation (Tsongas 1991, Straube 2011). This thermal effect decreases the vulnerability of the wall to water vapor migration from the interior carried either by air leakage or vapor diffusion. Different types of exterior insulation

materials vary in vapor permeability; mineral wool (MW), for example, is highly vapor-open whereas rigid foam insulation is typically vapor-tight. Vapor-tight exterior insulation may limit the outward drying potential of wall systems (Lstiburek 2013a, 2013b), although a small amount of air leakage between vapor-tight exterior insulation and the wood structural members may enhance outward drying potential (Lstiburek 2016).

A joint research project was initiated in 2014 by APA – The Engineered Wood Association and the USDA Forest Service, Forest Products Laboratory, to study the hygrothermal performance of split-insulated wall assemblies using a combination of different interior vapor retarders and continuous exterior insulation in the cold climate location of Madison, Wisconsin, USA. The project included field monitoring, laboratory measurements, and hygrothermal modeling. This report summarizes the field monitoring study. Also in this report, the background literature is reviewed and the study objectives are presented.

## 1.1 Previous Research

A considerable amount of field research has been conducted on moisture performance of wood-framed walls in cold climates (Glass and TenWolde 2007). A recent literature review by Trainor and Smegal (2017) focused specifically on various types of highly insulated walls (including walls with exterior insulation and double-stud walls) in North American cold climate locations. Several of the trends noted in this review are explored below.

Surveys and wall inspection studies generally have found no moisture problems with the use of exterior insulation. Wang (1981) inspected more than 70 houses during winter months, most of which were located in the Midwest and Northeast regions of the United States. No appreciable difference in moisture content (MC) was found between walls sheathed with extruded polystyrene, wood fiberboard, and plywood. In contrast, a survey of houses in the Northwest United States reported by Tsongas (1991) found that walls with exterior insulation had significantly lower wall moisture levels than walls without exterior insulation. In that study, some of the houses were in coastal Washington and the Seattle metropolitan area (marine climate) and some were in Montana (cold climate). Additional Canadian studies in various locations found that walls with extruded polystyrene sheathing did not have evidence of moisture accumulation in wood framing or evidence of interstitial condensation (Kane and Titley 1987, Proskiw 1995).

Multiple studies have investigated moisture performance of walls installed in conditioned test structures. Such studies have typically applied moisture loads to stress the walls, such as high interior relative humidity (RH), pressurization of the interior space to force exfiltration through wall assemblies, or intentional injection of a controlled amount of water at a known location. Additionally, some studies have included intentional deficiencies in the interior air barrier.

Many studies have concluded that adding exterior insulation does not increase the moisture-related durability risk (Sherwood 1983, Maref and others 2011, Smegal and others 2013, Fox and others 2014, Trainor and others 2016). An exception was noted by Trainor and Smegal (2017) for a subarctic climate (Fairbanks, Alaska; Climate Zone 8), for which the combination of intentional deficiencies in the interior polyethylene air–vapor barrier, high interior RH, and pressurization of the interior space resulted in wintertime moisture accumulation (Craven and Garber-Slaght 2012, 2014). Drying in spring and summer was significantly impeded for walls with low-permeance exterior insulation, thus increasing the moisture risk compared with walls with no exterior insulation. However, increasing the amount of exterior insulation such that 68% of the total thermal resistance was exterior of the plywood sheathing resulted in the lowest moisture risks. Exterior insulated walls without interior polyethylene had an appreciably faster drying rate in spring and summer than those with interior polyethylene.

In addition to low-permeance exterior foam insulation, several studies have monitored wall assemblies with high-permeance exterior MW insulation. Results indicate that walls with vapor-open exterior insulation allowed drying to the outside at a faster rate than walls with exterior foam insulation (Maref and others 2011, Fox and others 2014, Trainor and others 2016).

Conversely, several studies have found that low-permeance exterior insulation can decrease the inward flow of water vapor into the wall assembly from absorptive claddings such as brick veneer (Straube and Burnett 1998) and adhered stone veneer (Smegal and Grin 2015). In walls with these types of claddings (without low-permeance exterior insulation or another feature to decrease the inward vapor flow), an interior polyethylene vapor retarder has been shown to impede the inward vapor flow during summer conditions and to act as a condensing surface, resulting in condensed water running down and accumulating in the bottom plate (Wilkinson and others 2007).

The previously mentioned studies investigating moisture performance of walls with exterior insulation in cold climates have looked at a variety of wall configurations. Walls with 38- by 89-mm (nominal 2 by 4) framing have been studied with exterior insulation ranging from 0.88 $m^2 \cdot K/W$ (R-5) (Sherwood 1983, Smegal and Grin 2015) to as high as 4.1 $m^2 \cdot K/W$ (R-23) (Craven and Garber-Slaght 2012, 2014). Walls with 38- by 140-mm (nominal 2 by 6) framing have been monitored with 1.3 $m^2 \cdot K/W$ (R-7.5) (Smegal and others 2013) or 1.8 $m^2 \cdot K/W$ (R-10) exterior insulation (Maref and others 2011, Fox and others 2014, Trainor and others 2016). None of the previously mentioned studies has investigated 38- by 140-mm walls

with 0.88 $m^2$·K/W (R-5) exterior insulation, which meets the IECC prescriptive compliance path in cold climate zones (IECC Climate Zone 6 or higher). The objective of this study was to fill this gap.

### 1.2 Objectives

The overall goal of the project was to measure the moisture performance of 38- by 140-mm wood-framed wall assemblies with and without exterior insulation in a cold climate location. Specific objectives were to characterize wall assembly moisture and temperature conditions under ambient environmental conditions with low and high interior moisture load conditions and to characterize wall assembly drying rates after intentional wetting of the wood structural panel sheathing. The primary variables included in the study were the following:

- Type of exterior insulation: none, MW, expanded polystyrene, or extruded polystyrene
- Type of interior vapor retarder: polyethylene sheet or asphalt-coated kraft paper
- Interior moisture load levels: wintertime RH of 42% (first year) and 34% (second year)

## 2 Methods

### 2.1 Description of Test Structure

The test structure was an existing building located at the Valley View test site of the USDA Forest Service, Forest Products Laboratory. This location just west of Madison, Wisconsin, USA, has been used for many outdoor experiments (Duff 1968, Sherwood 1983, TenWolde and others 1995, Carll and others 2013) to represent a cold climate, specifically IECC Zone 6 (Baechler and others 2010). The 17.2- by 4.9-m building has a treated wood post and beam foundation, which raises it off the ground. The insulated floor was not changed, but the 38- by 140-mm stud walls of the original building were refurbished to create test sections (Fig. 2), and the ceiling was insulated with cellulose fiber to facilitate conditioning of the interior. The long dimension of the building runs east to west with a central room and a wing on each end. The central room, which houses the data acquisition system and heating and cooling equipment, has a door on the north side. Existing siding, building paper, insulation, vapor retarder, and gypsum board were removed from the north and south walls of the wings, and these walls were subsequently all sheathed with 11-mm oriented strandboard (OSB) purchased at a local building supply store. Each 1.2-m-wide by 2.2-m-high test section, consisting of three cavities with studs 406 mm (16 in.) on center, was separated from adjacent wall sections using a plastic composite trim board on the outside (to keep the OSB panels from touching) and by adding an additional 38- by 140-mm stud separated from the existing studs using an impermeable self-adhering membrane. Test sections were thus isolated to minimize any moisture transfer between adjacent wall sections. Figure 3 shows a plan view with 16 test sections. The outside walls were covered with spun-bonded polyolefin house wrap (Fig. 4) and exterior insulation (depending on the assembly, as subsequently described), and vinyl siding was installed (Fig. 5). The 140-mm stud cavities were filled with fiberglass batt insulation that had nominal thermal resistance of 3.7 $m^2$·K/W (R-21). The interior was finished with 12.7-mm gypsum board, latex primer, and latex paint.

**Figure 2. Northeast corner of test structure undergoing partial reconstruction.**

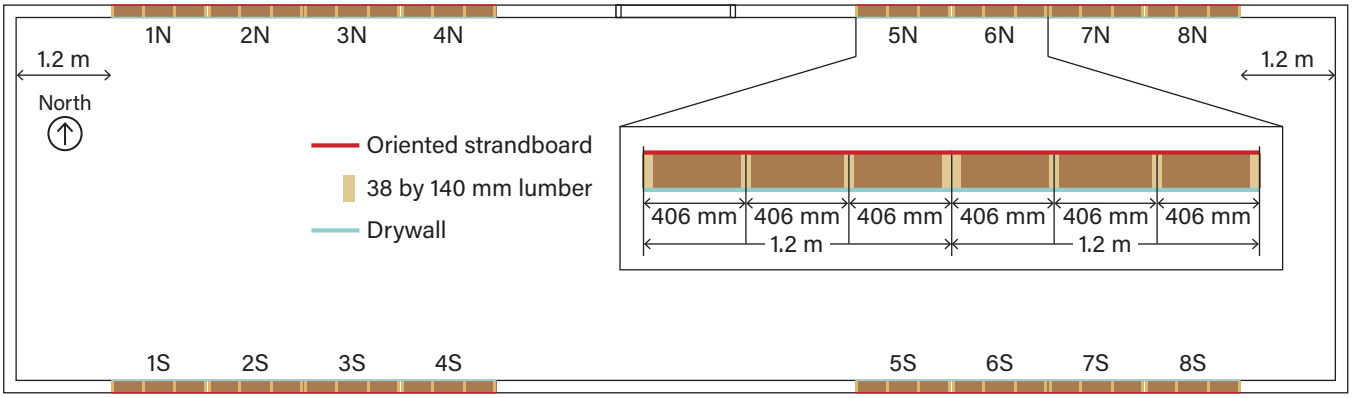


**Figure 3. Plan view of test structure showing 16 test sections.**


**Figure 4. Northwest corner of test structure before installation of exterior insulation. The right-most section is not an instrumented section.**

**Figure 5. Completed south side of the test structure.**


**Figure 6. Northwest interior corner of test structure with wall cavities insulated before drywall installation (CI, continuous insulation; MW, mineral wool).**

The interior of the building was temperature controlled with an electric furnace during winter (20 °C heating set point) and an air conditioner during summer (25.6 °C cooling set point). Humidity levels were maintained in the winter using a humidistat (42% RH first winter and 34% RH second winter) and associated atomizer in each of the wings. There was no separate dehumidification in summer beyond that provided by operation of the air conditioner under thermostat control. Fans circulated air within each wing and between wings to promote uniform temperature and humidity conditions within the building.

## 2.2 Wall Configurations

Each of the eight different test sections had an identical configuration for north and south (aside from orientation). As previously mentioned, all wall sections included vinyl siding, house wrap, OSB sheathing, fiberglass cavity insulation, and interior gypsum drywall. All wall sections had gasketing installed between the framing and drywall for airtightness. Figure 6 shows the insulated walls before the drywall installation in the northwest section. Test sections had varied combinations of interior vapor retarder and exterior insulation (outboard of the OSB and house wrap) to implement a split-insulated wall design similar to Figure 1.

Walls 1 and 2 (numbered west to east) were the base case without any exterior insulation and differed only by the internal vapor retarder, which was the asphalt-coated kraft paper facing of the fiberglass insulation in Wall 1 and a 0.15-mm polyethylene sheet in Wall 2.

Walls 3 and 4 repeat this pattern but included 38 mm of MW exterior insulation to add 1.1 $m^2 \cdot K/W$ (R-6) to the configuration.

Wall 5 used 38 mm of expanded polystyrene (EPS) paired with the kraft interior to provide 1.1 $m^2 \cdot K/W$ (R-6).

Walls 6 and 7 were both 25.4 mm of extruded polystyrene (XPS) paired with kraft and polyethylene interior vapor retarders, respectively, to provide 0.88 $m^2 \cdot K/W$ (R-5).

Wall 8 was again 25.4 mm of XPS and kraft interior, but the house wrap was not the flat spunbond polyolefin fiber used in all the other walls. Instead, Wall 8 used a similar product structured to create a vertically grooved surface that promotes water drainage, which resulted in a small air gap between the sheathing and the XPS.

Table 1 shows all eight different configurations.

**Table 1—Wall configuration summary**

| Wall | Interior vapor retarder | House wrap | Exterior insulation | Label[a] |
|---|---|---|---|---|
| 1 | Kraft paper | Flat polyolefin | None | No CI, kraft |
| 2 | Polyethylene | Flat polyolefin | None | No CI, poly |
| 3 | Kraft paper | Flat polyolefin | 38-mm mineral wool | MW, kraft |
| 4 | Polyethylene | Flat polyolefin | 38-mm mineral wool | MW, poly |
| 5 | Kraft paper | Flat polyolefin | 38-mm expanded polystyrene | EPS, kraft |
| 6 | Kraft paper | Flat polyolefin | 25.4-mm extruded polystyrene | XPS, kraft |
| 7 | Polyethylene | Flat polyolefin | 25.4-mm extruded polystyrene | XPS, poly |
| 8 | Kraft paper | Crinkled polyolefin | 25.4-mm extruded polystyrene | XPS, kraft, crinkled |

[a]CI, continuous insulation; MW, mineral wool; EPS, expanded polystyrene; XPS, extruded polystyrene.

## 2.3 Instrumentation

The test hut walls were instrumented with a focus on the MC of the OSB sheathing. Each test section had an identical set of sensors, which were always installed in the middle cavity (of the three that make up a section). That central cavity was caulked between the OSB and framing to decrease air infiltration. Wiring to the sensors went through the framing to an adjacent cavity in the section and was also caulked at that framing penetration. Each section included six paired sensors that combined a moisture pin pair (measuring resistance to calculate MC) and thermistor (measuring resistance to calculate temperature). The moisture pin pair was not the traditional driven nail. Instead, the connection to the OSB for the resistance measurement was accomplished using 18-8 stainless steel sheet metal screws (slotted hex washer head, #6 x 12.7 mm), which then contacted the point moisture measurement (PMM) sensor (SMT Research Ltd., Vancouver, British Columbia, Canada) that also housed the thermistor (MF58104F3950, Cantherm, Montreal, Quebec, Canada). Such a moisture pin system has been studied in OSB by Boardman and others (2017) and provides good long term contact with the OSB. Leads from the moisture pin and thermistor connected to a wireless 8-channel data acquisition (DAQ) unit that read and stored the resistance measurements (A3, SMT Research Ltd.). Each wireless DAQ unit communicated to a central hub running display and storage software (Building Intelligence Gateway, SMT Research Ltd.) on a laptop computer. Data were collected once per hour. The DAQ unit read resistance with accuracy of ±5% up to a maximum of 1 GΩ. When combined with the thermistor error, this led to an uncertainty in temperature readings of at most 1.2 °C. When combined with the uncertainty of the OSB resistance to MC correlation, this led to an uncertainty in MC of at most 1.3%. However, very low MC (below around 8%) had large errors because the recorded resistance has a maximum value of 1 GΩ.

Two of the PMM sensors measured structural lumber, whereas four were in the OSB (Fig. 7). PMM4 was in the bottom plate capturing MC (MC4) and temperature (T4). PMM2 was in the 38- by 140-mm structural lumber near the middle of the cavity (1.14 m up from the bottom plate). PMM1 was in OSB 100 mm down from top plate, whereas PMM3 was 100 mm up from bottom plate. PMM5 and PMM6 were in the field of a shop towel used for water injections, which will be subsequently discussed. PMM5 was 1.17 m up from bottom plate, whereas PMM6 was 100 mm below PMM5. All the MC measurements in OSB were calculated from the resistance measurements using the formula in Boardman and others (2017), which describes the efforts to improve correlation of MC with resistance and temperature data in OSB. The A3 DAQ units were mounted in an adjacent cavity.

From the OSB MC and temperature measurements, an "apparent surface RH" value was calculated using a generic OSB sorption isotherm relation based on data sources outlined in Boardman and others (2017) and described in Appendix A. In addition to the combined MC and temperature measurements, two other sensors recorded RH and temperature in the cavity. One was a Humirel HTS2010 sensor that connected to the SMT A3 system. It was placed just below MC1 as shown in Figure 8 to record conditions near the OSB capturing RH (RH7) and temperature (T7). This humidity sensor had accuracy of ±3% to ±5% RH. The other RH sensor was placed near MC2 to capture overall conditions in the cavity at midheight (RH8, T8). That system was an independent data logger (HOBO U23-002 Pro v2 External Temperature/RH Logger, Onset Computer Corporation, Bourne, Massachusetts, USA), which also logged once per hour. The HOBO humidity sensor also had accuracy between ±3% to ±5% RH, with temperature accuracy of 0.21 °C.

Both indoor and outdoor RH and temperature were measured using HMP233 sensors (Vaisala, Vantaa, Finland), which output 0–5 volt signals read by an Adam 6017 analog input module (Advantech Co., Ltd., Taipei, Taiwan) with custom software recording once per hour. The Vaisala units had accuracy of ±1% RH and ±0.2 °C. Local wind conditions were measured on top of a 7.6-m fiberglass tower using a Gill WindSonic (Gill Instruments

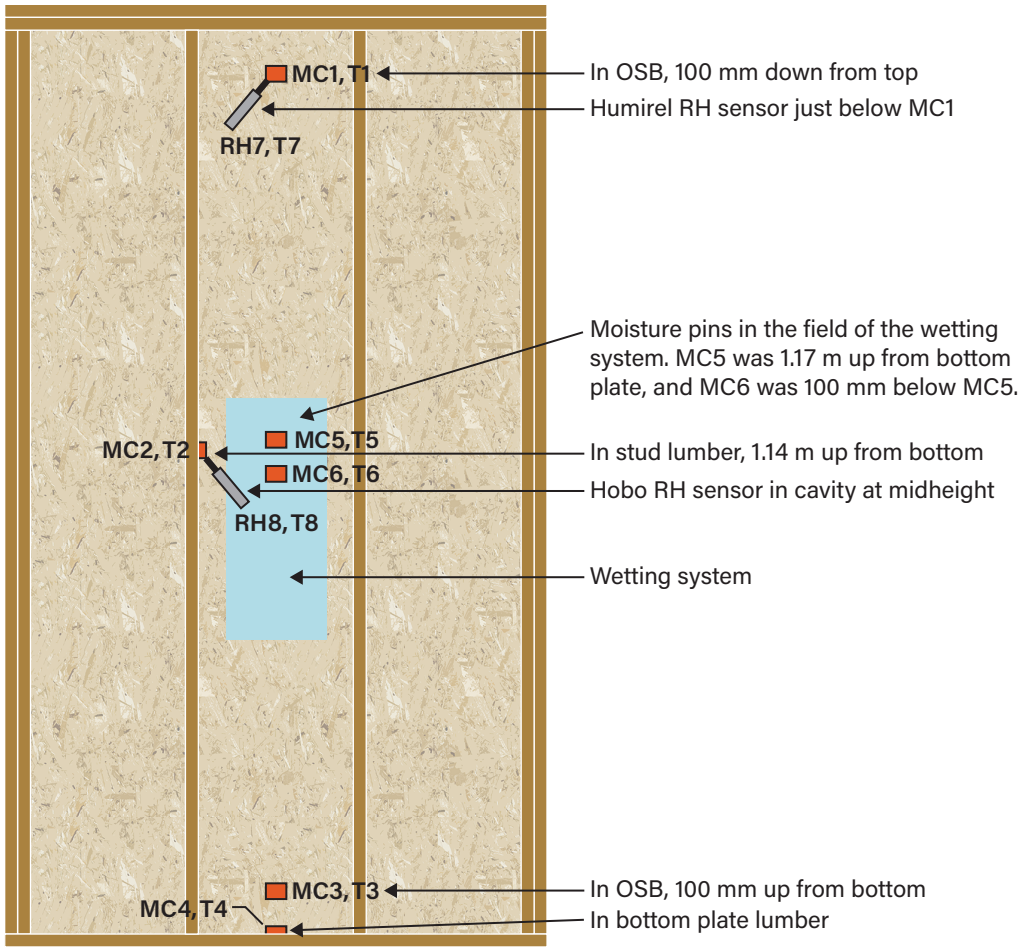


**Figure 7. Sensor placement in each test section (OSB, oriented strandboard; RH, relative humidity).**

**Figure 8. Instrumentation at top of cavity recording moisture content, relative humidity, and temperature.**

Limited, New Milton, UK) with data captured every 2 s and averaged to yield hourly average wind speed and direction. Local rainfall was measured using a tipping bucket (Series 525 rainfall sensor, Texas Electronics, Dallas, Texas, USA) with each tip recorded on the EL-USB-5 counter (Lascar Electronics Ltd., Salisbury, England). Both the rain and wind sensors were located in an open area more than 7.6 m from the test facility. Solar radiation was not measured directly on site but was taken from a Madison, Wisconsin, station maintained by the National Oceanic and Atmospheric Administraton's Earth System Research Laboratory through the SOLRAD network (https://www.esrl.noaa.gov/gmd/grad/solrad/index.html).

### 2.4 Water Injections

To provide a drying challenge to the wall systems, each cavity was subjected to an identical water injection schedule at three different times during the 2-year study. The wetting occurred inside the center cavity using a 3.1-mm inner diameter vinyl tube that allowed water to flow from the indoor entry point near the drywall surface to the OSB inside surface behind the fiberglass insulation where the water was held in place by a shop towel (Van Straaten 2003). Three small holes in the tube allowed a trickle of water to enter the paper shop towel stapled to the OSB surface. This wetting system has been found to yield consistently reproducible wetting of a localized OSB area and to promote OSB water absorption. Each injection had a volume of 40 mL, which wet the shop towel without running down the OSB sheathing. Figure 9 shows the tube and towel system installed with MC5 and MC6 in the field of the shop towel. The shop towel was cut out around the sensors, which allowed the screws for MC measurement to go directly into the OSB without touching the shop towel.

The first series of injections occurred in late summer, starting August 13, 2015, with one injection per day for 3 days (total of 120 mL). The second series of injections occurred in late fall, starting November 6, 2015, and lasted 5 days (total of 200 mL). The last series of injections occurred the following spring, starting May 20, 2016, and lasted 4 days (total of 160 mL).

## 3 Results

### 3.1 Interior and Exterior Environmental Conditions

Outdoor temperatures were similar to 1981–2010 averages recorded at the KMSN weather station (Madison, Wisconsin, airport) for the 2-year study, but the relative humidities were higher than average. Figure 10 shows a weekly plot of recorded outdoor temperature along with the 30-year normal. Figure 11 shows a weekly plot of recorded outdoor humidity along with the 30-year normal. The number of heating degree days (65 °F basis) recorded at the KMSN weather station averaged 7,333 for the 1981–2010 period, whereas somewhat lower than normal values were recorded for the study years with 6,667 (91% normal) in 2015 and 6,417 (88% normal) in 2016. Calculated heating degree days using recorded temperatures at the test site were slightly (less than 1%) higher than the KMSN weather station values.

Similarly, precipitation was above average, particularly in the second year. Figure 12 shows the cumulative precipitation by month.

Indoor temperatures were moderated by the heating and air conditioning systems to typical interior conditions. Figure 13 shows the indoor weekly temperatures compared

**Figure 9. Water injection system.**

with outdoor for the full 2 years, whereas Figure 14 shows the same data at an hourly level for the summer to illustrate exterior conditions cycling above interior during parts of the day.

Similarly, indoor RH levels were moderated by the humidifier during the winter and air conditioning during the summer. Figure 15 shows the weekly indoor and outdoor RH averages.

Inspection of Figure 15 reveals that the winter RH set point was higher the first winter (near 42% RH) than the second winter (near 34% RH). Figure 16 shows the difference between indoor and outdoor vapor pressure during the whole period. The indoor vapor pressure was higher than outdoors in winter but less than outdoors in summer. The equation used for saturation vapor pressure (Pws) needed to calculate indoor vapor pressure is slightly modified from Buck (1981) with output in pascals given temperature $t$ in °C:

$$\mathrm{Pws} = 613.65e^{\left[\left(\left(18.729-\left(\frac{t}{227.3}\right)\right)t\right)/(t+257.87)\right]} \quad (1)$$

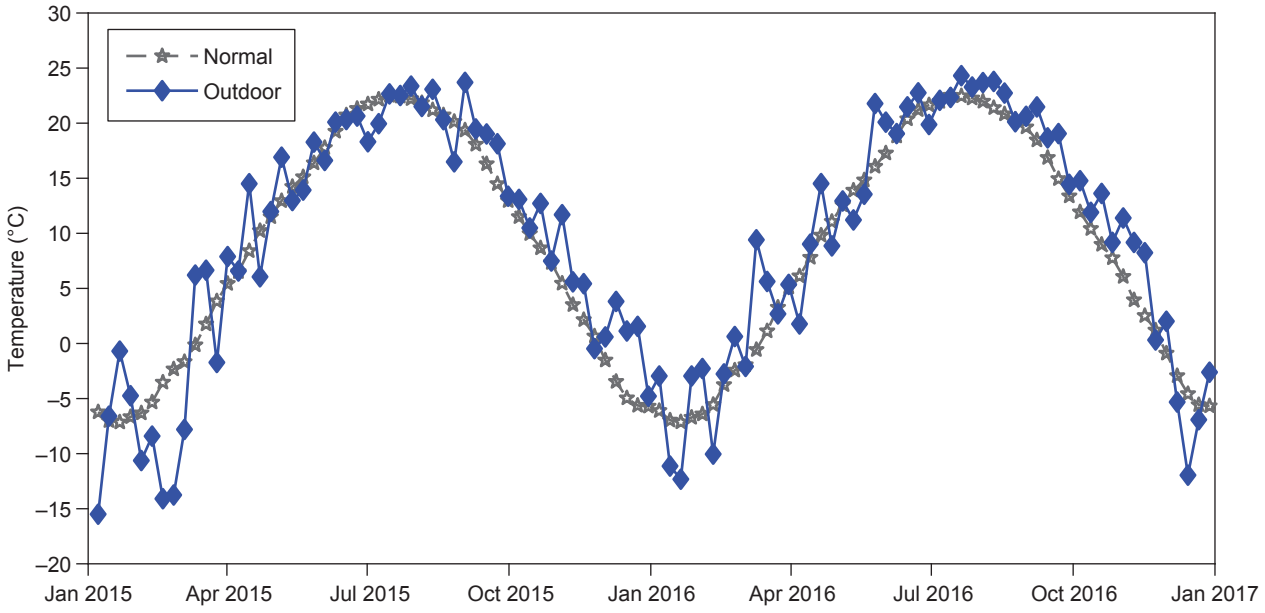


**Figure 10. Weekly average outdoor temperatures compared with 30-year normal.**

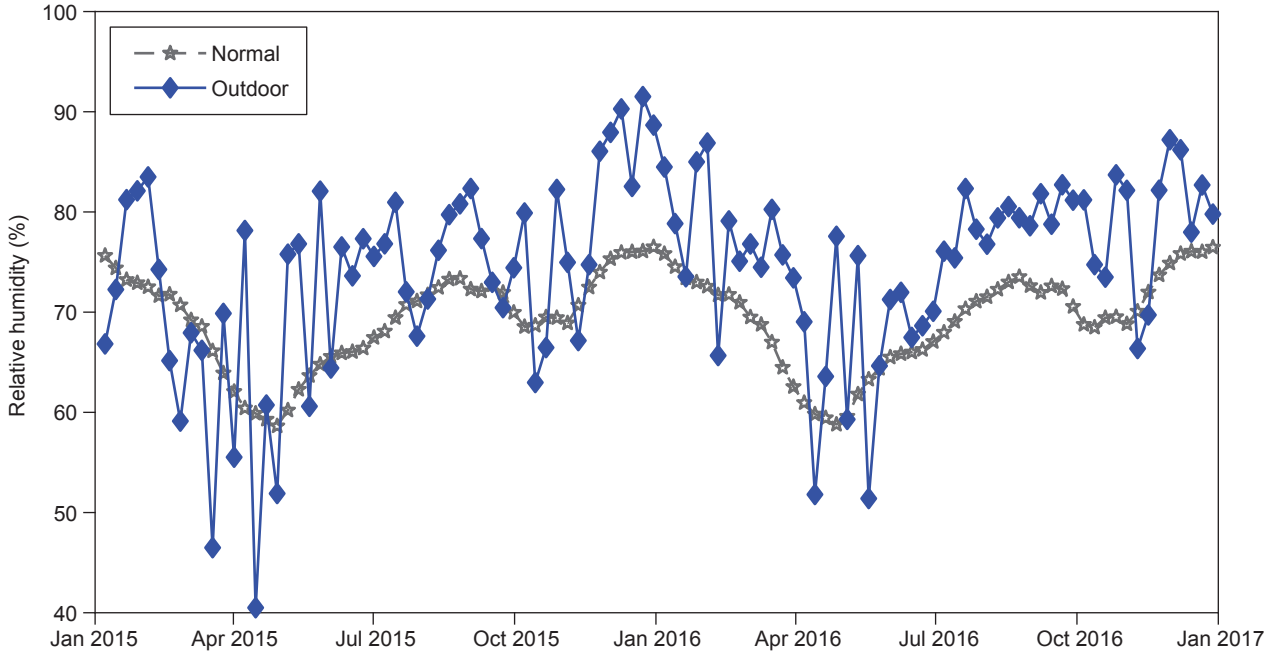


**Figure 11. Weekly average outdoor relative humidity compared with 30-year normal.**

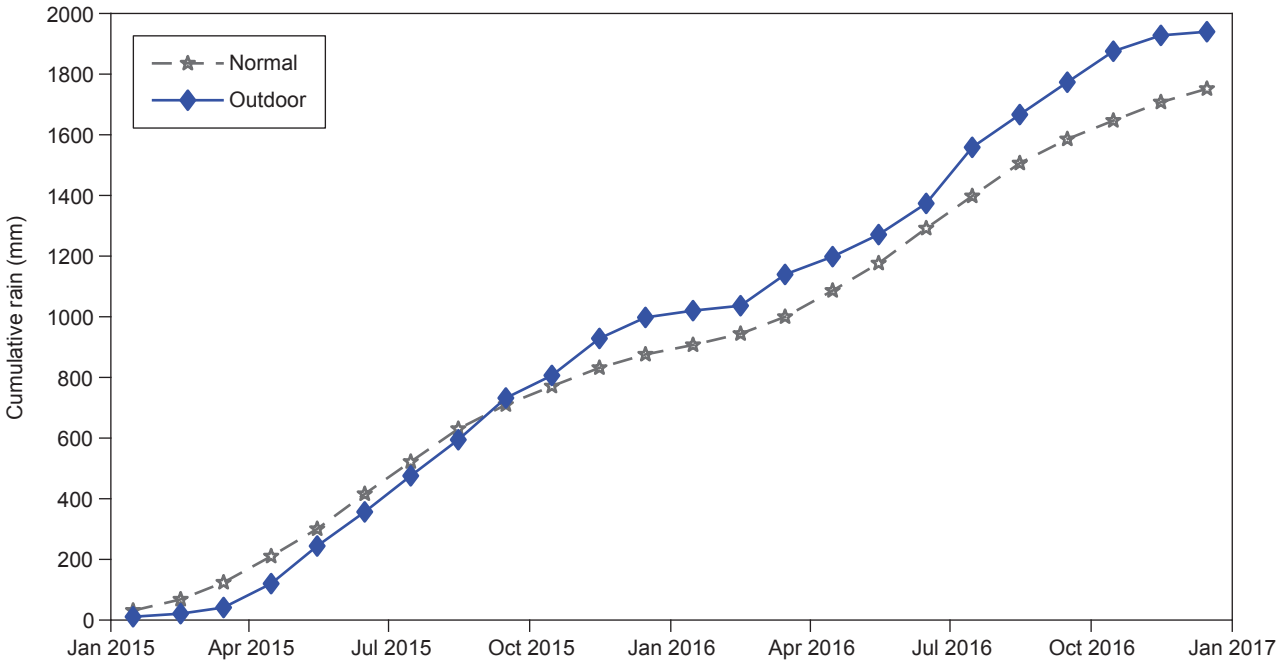


**Figure 12. Cumulative precipitation compared with 30-year normal.**

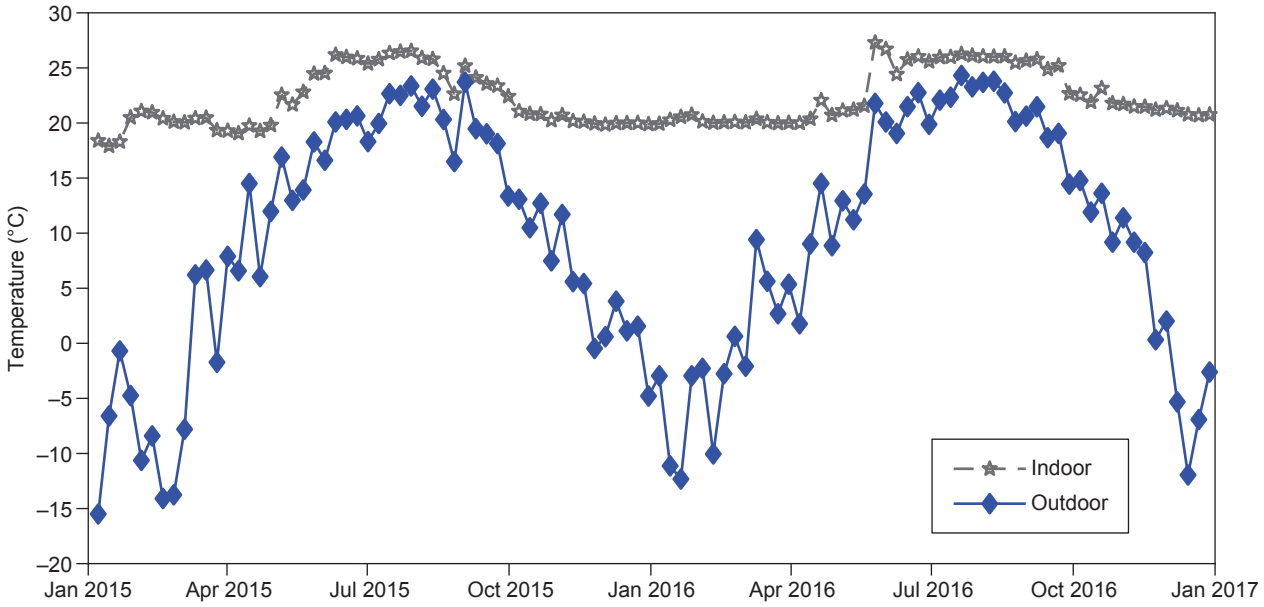


**Figure 13. Weekly average indoor and outdoor temperatures.**

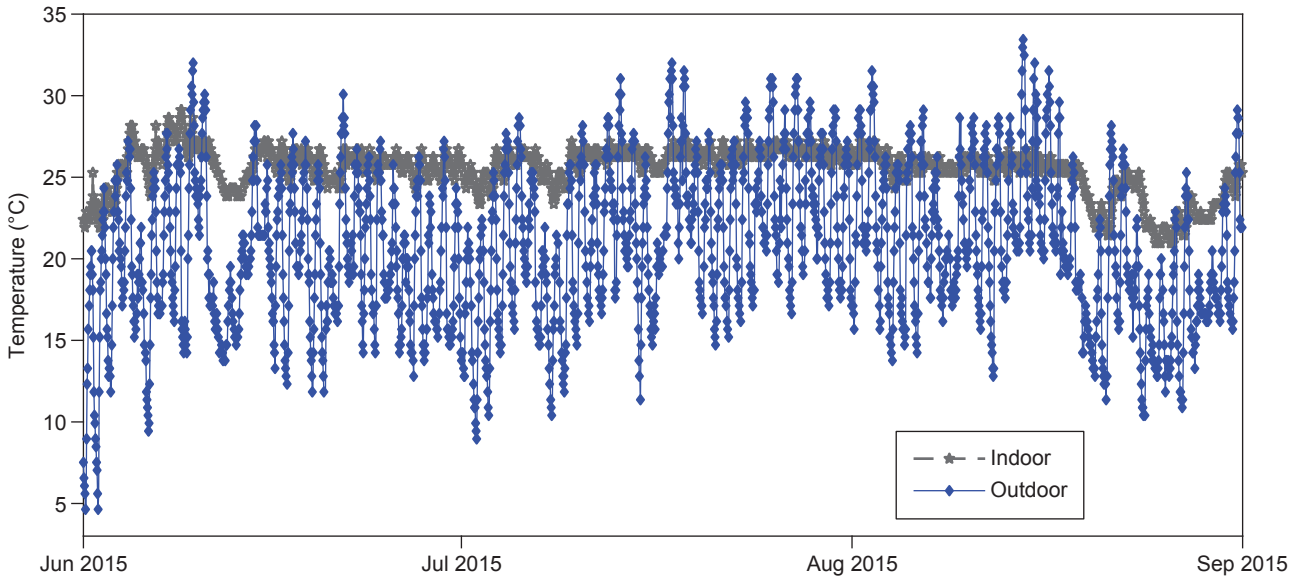


**Figure 14. Hourly indoor and outdoor temperatures during summer.**

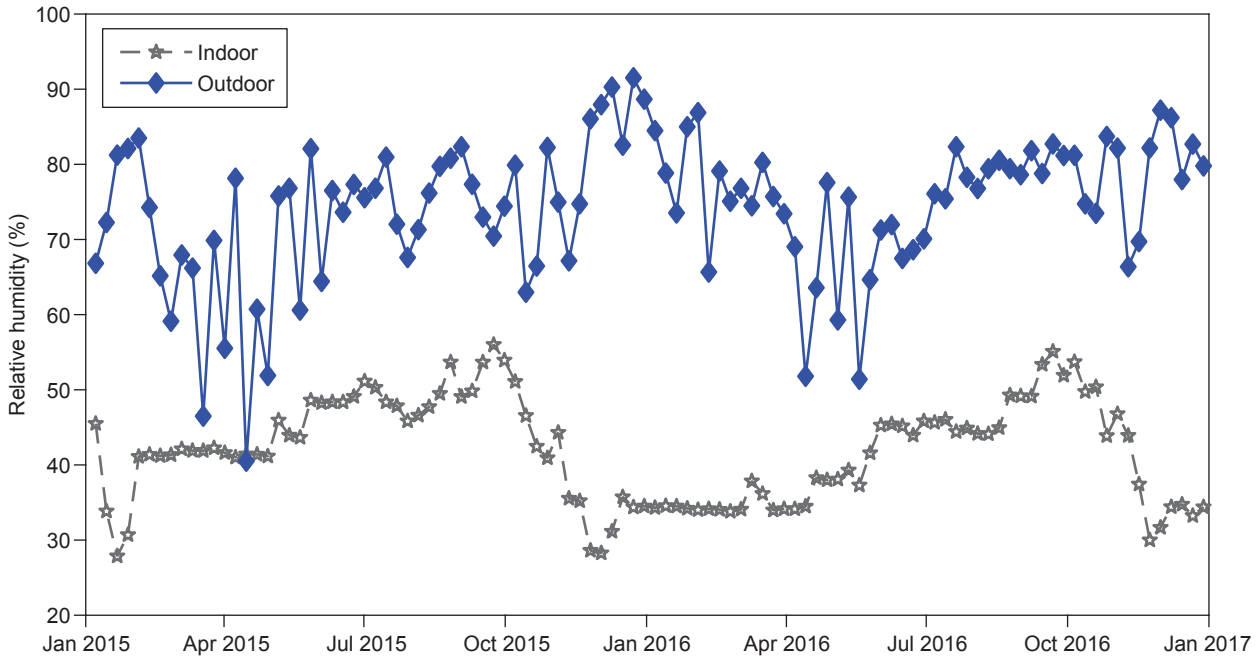


**Figure 15. Weekly average indoor and outdoor relative humidity.**

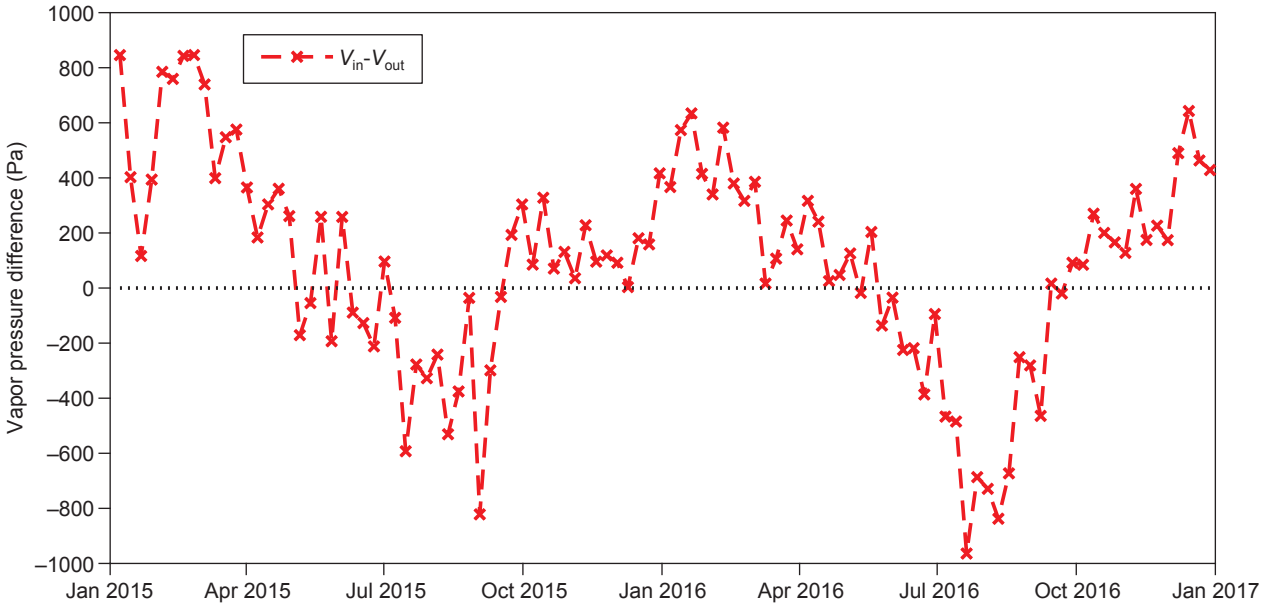


**Figure 16. Indoor–outdoor vapor pressure difference.**

## 3.2 Wall Assembly Temperatures

Temperatures of the OSB inside each cavity unsurprisingly tracked outdoor temperatures. Figure 17 shows the weekly average of T1, 100 mm down from the top plate, for all north walls. Inspection of Figure 17 shows that, during winter, the OSB was colder when there was no exterior insulation.

Most temperature sensors also picked up the expected vertical stratification inside the wall cavity. Figure 18 illustrates this in Wall 2 north (no continuous insulation (CI), poly) by plotting T1 (near top plate) with T6 (lower in the cavity). However, the difference was small and usually below the uncertainty in temperature measurement. Also against the expected trend, Wall 5 north (EPS, kraft) showed T1 at a lower temperature than T6 when averaged across the whole 2-year period. Similarly, the south walls were slightly warmer than the north walls as shown in Figure 19, which plots T1 for Wall 2 (no CI, poly) north and south. Again, the difference was usually below the uncertainty in temperature measurement, but in this case, all walls showed south warmer than north.

Finally, for a quantitative comparison of the effects of the exterior insulation, Table 2 reports the average temperature difference between T7 (Humirel sensor close to inside surface of OSB at top) and outdoors during the winter months, December 2015 through February 2016. Each wall type reported includes the average of both north and south walls.

**Table 2—Average temperature difference between oriented strandboard and outdoors for north and south walls during winter**

| Wall | Label[a] | Temperature difference (°C) |
|---|---|---|
| 1 | No CI, kraft | 3 |
| 2 | No CI, poly | 4 |
| 3 | MW, kraft | 8 |
| 4 | MW, poly | 9 |
| 5 | EPS, kraft | 7 |
| 6 | XPS, kraft | 7 |
| 7 | XPS, poly | 8 |
| 8 | XPS, kraft, crinkled | 7 |

[a]CI, continuous insulation; MW, mineral wool; EPS, expanded polystyrene; XPS, extruded polystyrene.

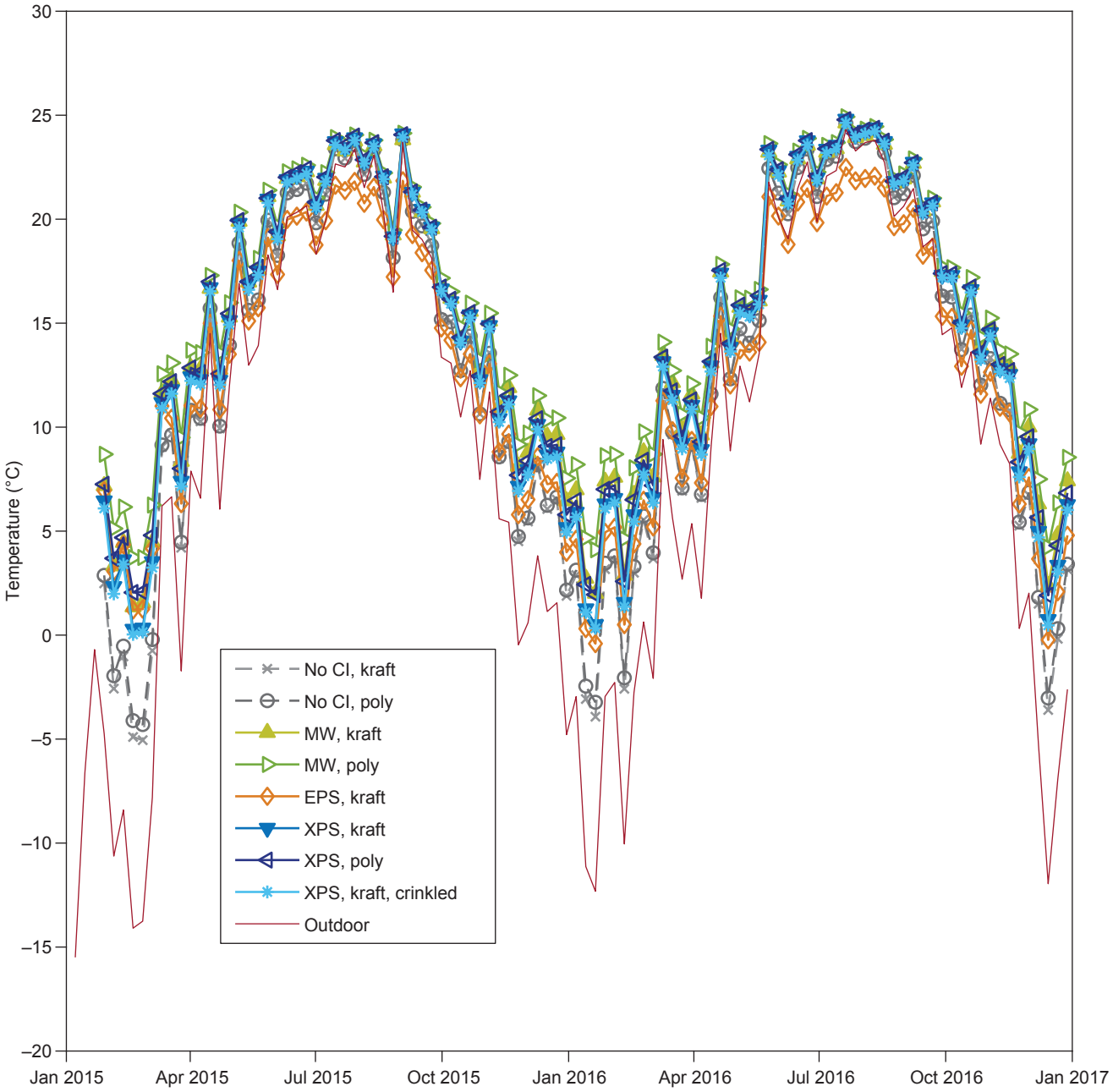


**Figure 17. North wall temperatures in oriented strandboard near top plate (CI, continuous insulation; MW, mineral wool; EPS, expanded polystyrene; XPS, extruded polystyrene).**

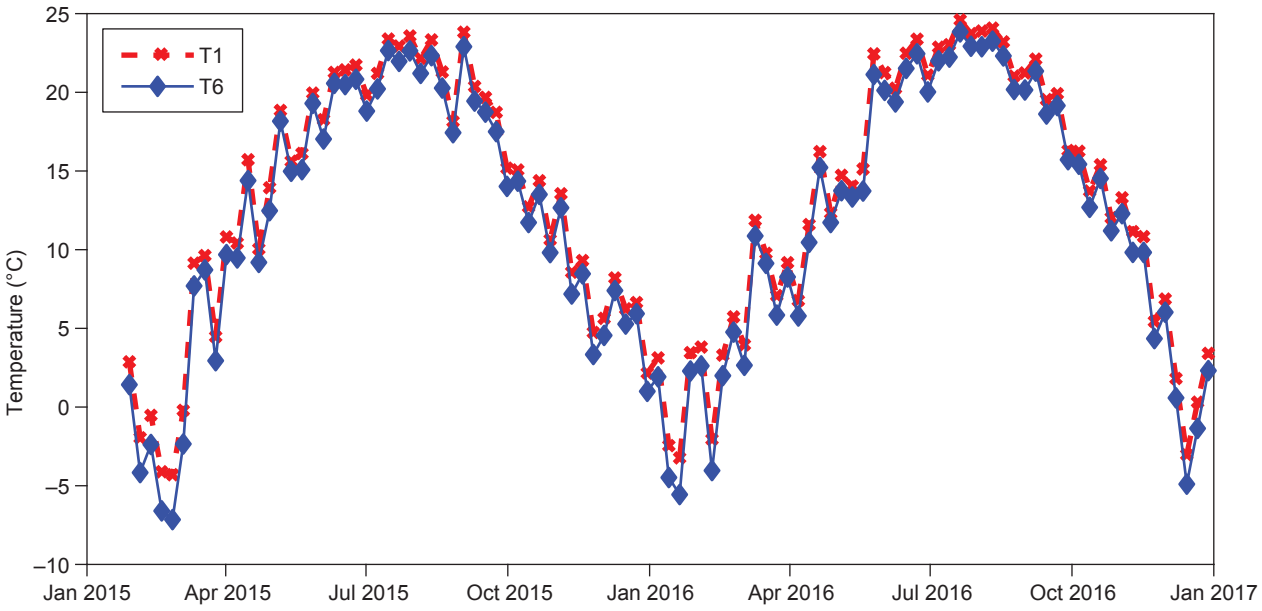


**Figure 18. North, no CI, poly wall showing temperature stratification (CI, continuous insulation).**

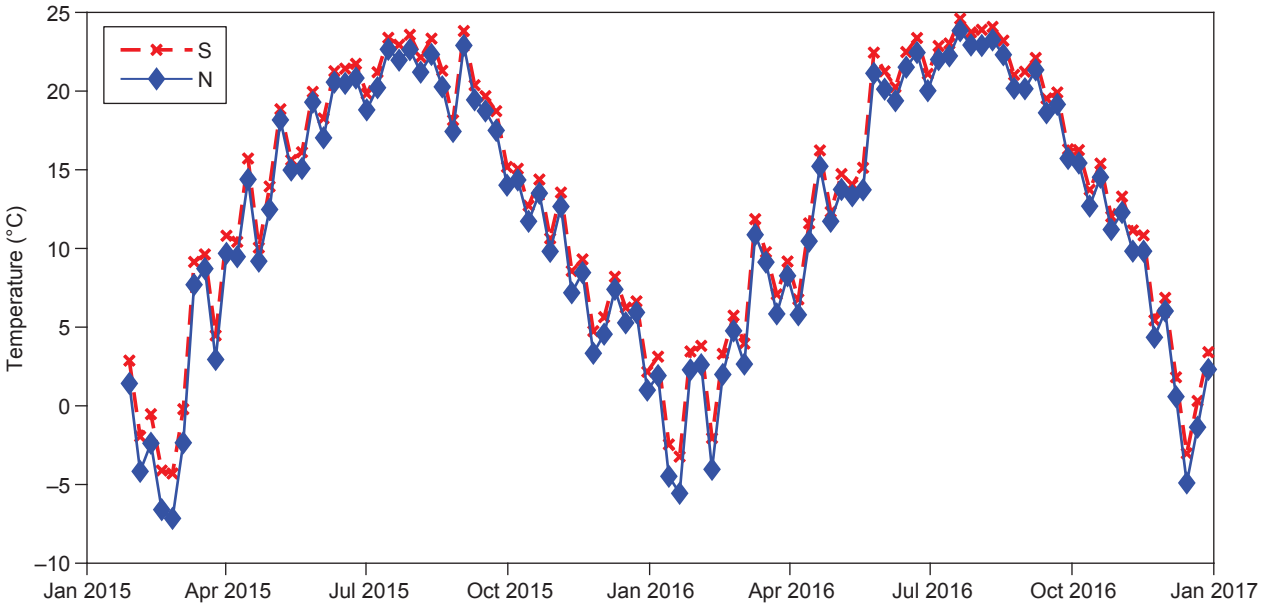


**Figure 19. T1, no CI, poly wall showing south (S) warmer than north (N) (CI, continuous insulation).**

## 3.3 Vapor Pressures

Vapor pressures inside each cavity typically fell between the indoor and outdoor boundary conditions. Figure 20 illustrates this by plotting the weekly average vapor pressure calculated using Equation (1) from the RH and temperature readings of the HOBO sensor (midheight in the cavity at mid-depth) for the two base case north walls along with indoor and outdoor conditions. Generally, the cavity with kraft vapor retarder was closer to indoor conditions. All the north wall cavity weekly average vapor pressures are plotted in Figure 21, which shows that the cavities with polyethylene vapor barrier had higher vapor pressure than cavities with kraft in summer and generally had lower vapor pressure than kraft cavities during winter. Figures 20 and 21 also show the timing of the water injections with the red bar at the bottom.

Figure 22 is a plot of daily average vapor pressures in two north wall cavities after the first injection. During August and September 2015, the outdoor vapor pressure was generally greater than indoor vapor pressure and the cavity vapor pressures were typically in between, indicating an inward vapor drive. It is unclear if the increase in cavity vapor pressure after the water injection was a result of the injection or the rise in outdoor vapor pressure. There were brief windows after the injection in which the cavity vapor pressures rose above both indoor and outdoor vapor pressure, indicating that drying was occurring in both directions. This effect was greater and lasted longer when there was exterior insulation. Although the difference between MW and no-CI walls was not larger than the measurement error in Figure 22, it was often significant in Figure 23, which plots the daily average vapor pressures for the second injection. In Figure 23, there are longer periods during which the wall was drying in both directions. This injection occurred during colder weather, and the outdoor vapor pressure fluctuated above and below indoor vapor pressure during November and December.

Also shown in Figure 23 is the vapor pressure at the surface of the OSB compared with the HOBO sensor for one cavity, the north MW, kraft. In general, these tracked closely, but right after the injection, the OSB surface conditions were wetter than the overall cavity. The surface vapor pressure was calculated using the M5 moisture pin (in field of wetting system) and the apparent surface RH from an OSB sorption isotherm (Appendix A). That surface RH was then combined with the surface temperature to calculate surface vapor pressure. The same trends can be seen during the third injection shown in Figure 24, which occurred during mild spring weather.

For a different way to compare the eight wall types, the following calculation was made with hourly values to show the average vapor pressure difference between each cavity and outdoors. The cavity vapor pressure was the average of the Humirel sensor (RH7, T7) near the OSB and the HOBO sensor midcavity. North and south values were averaged for each wall. These values were normalized by subtracting the outdoor vapor pressure. Finally, the hourly values were averaged across time into three bins: 5 weeks before an

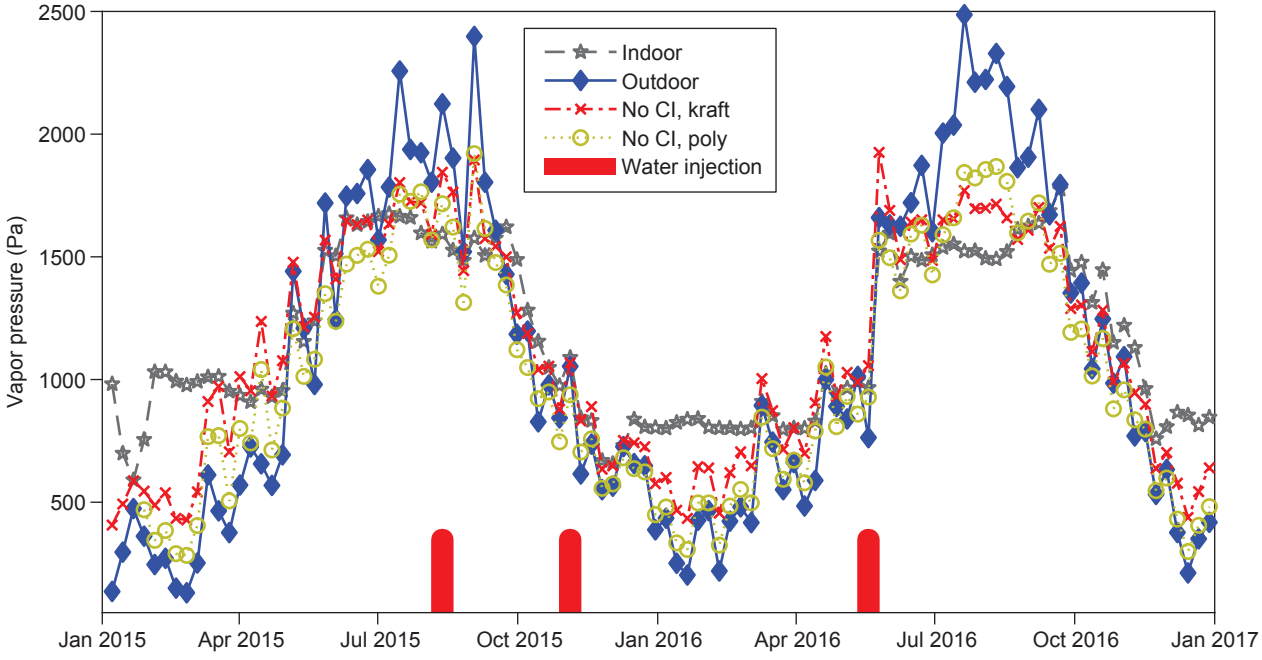


**Figure 20. Vapor pressure in two north wall cavities compared with indoor and outdoor conditions (CI, continuous insulation).**

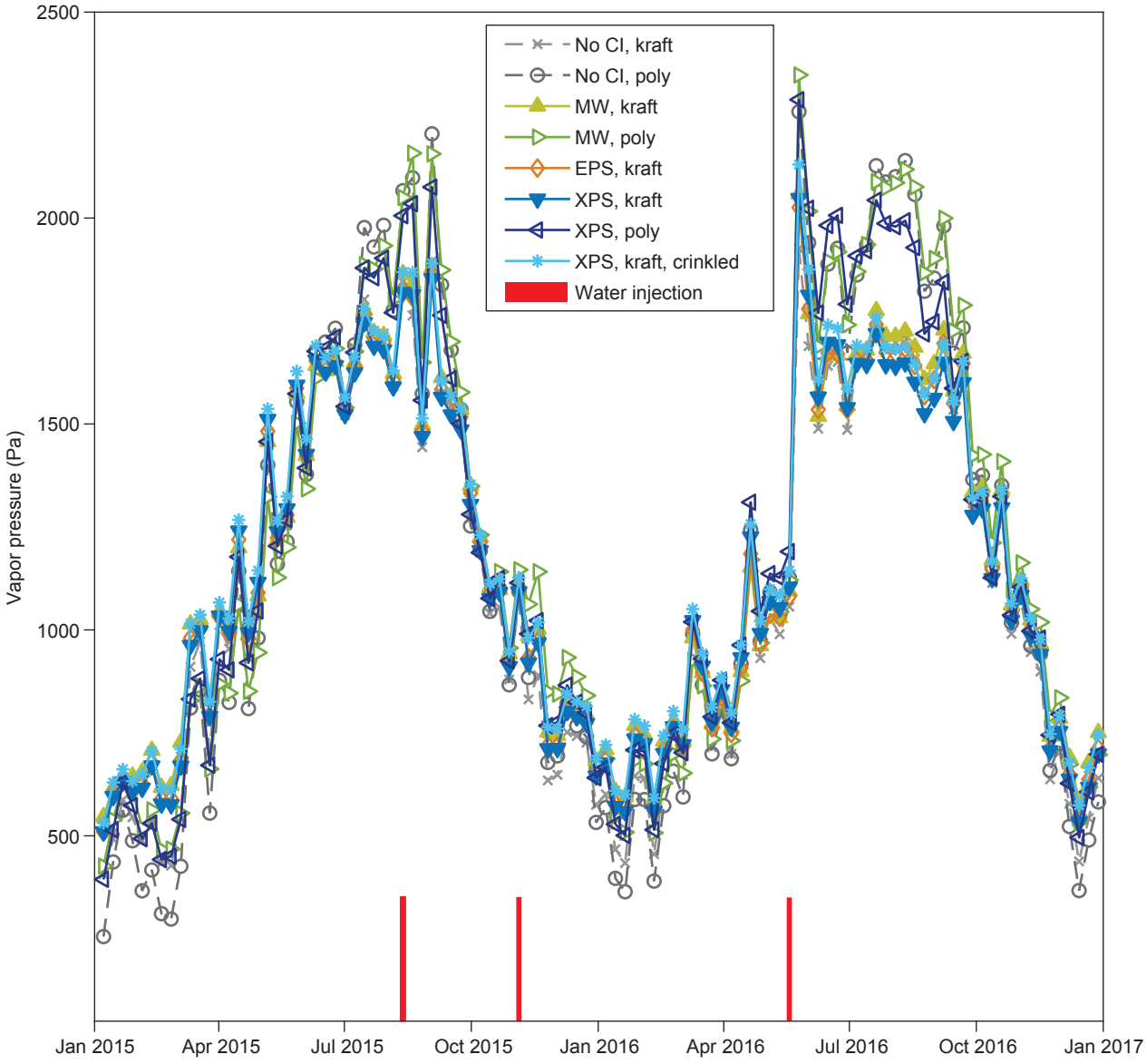


**Figure 21. Vapor pressure for all north cavities (CI, continuous insulation; MW, mineral wool; EPS, expanded polystyrene; XPS, extruded polystyrene).**

injection, 1 week after injection, and weeks 2–5 following injection. These averages for each injection are shown in Table 3 for all eight walls.

Prior to the first injection, all wall cavities were at lower vapor pressure than outdoors. This injection coincided with an increase in cavity vapor pressure in the first week, followed by a decrease in weeks 2–5. The rise in cavity vapor pressure was most pronounced for the walls with interior polyethylene (Walls 2, 4, and 7), and these walls also had considerably higher cavity vapor pressures than the other walls prior to the injections, which is consistent with the interior polyethylene impeding inward drying. Prior to the second injection, all wall cavities were slightly above outdoor vapor pressure. The largest increase in cavity vapor pressure in the week after this injection was in Walls 4 and 7, which also remained higher than the other walls in weeks 2–5. Following the third injection, all wall cavities had a downward trend in vapor pressure relative to outdoors except for the walls with interior polyethylene (Walls 2, 4, and 7).

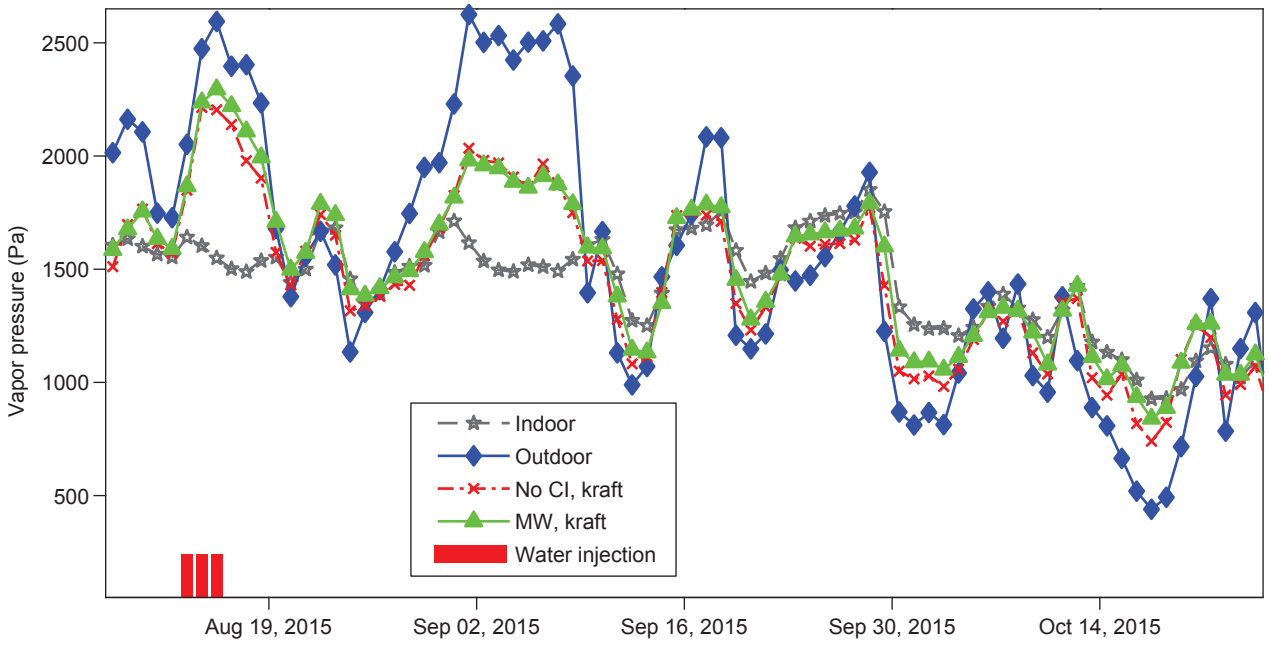


**Figure 22. Daily average vapor pressure after Injection 1 (CI, continuous insulation; MW, mineral wool).**

**Table 3—Average vapor pressure difference between cavity and outdoors**

| | | Vapor pressure difference (Pa) | | | | | | | | |
|---|---|---|---|---|---|---|---|---|---|---|
| | | Injection 1 (August 2015) | | | Injection 2 (November 2015) | | | Injection 3 (May 2016) | | |
| Wall | Label[a] | 5 weeks pre | 1 week post | 2–5 weeks post | 5 weeks pre | 1 week post | 2–5 weeks post | 5 weeks pre | 1 week post | 2–5 weeks post |
| 1 | No CI, k | –282 | –230 | –243 | 52 | 123 | 36 | 137 | –19 | –172 |
| 2 | No CI, p | –151 | –12 | –88 | 38 | 157 | 64 | 114 | 118 | –37 |
| 3 | MW, k | –334 | –236 | –266 | 56 | 166 | 81 | 64 | –46 | –218 |
| 4 | MW, p | –226 | 2 | –106 | 47 | 242 | 161 | 25 | 115 | –87 |
| 5 | EPS, k | –335 | –245 | –280 | 52 | 150 | 72 | 94 | –23 | –202 |
| 6 | XPS, k | –362 | –297 | –313 | 51 | 136 | 71 | 127 | –16 | –199 |
| 7 | XPS, p | –232 | –61 | –154 | 62 | 212 | 125 | 169 | 195 | 42 |
| 8 | XPS, k, cr | –359 | –273 | –312 | 49 | 148 | 78 | 130 | 15 | –187 |

[a]CI, continuous insulation; MW, mineral wool; EPS, extruded polystyrene; XPS, expanded polystyrene; k, kraft; p, polyethylene; cr, crinkled.

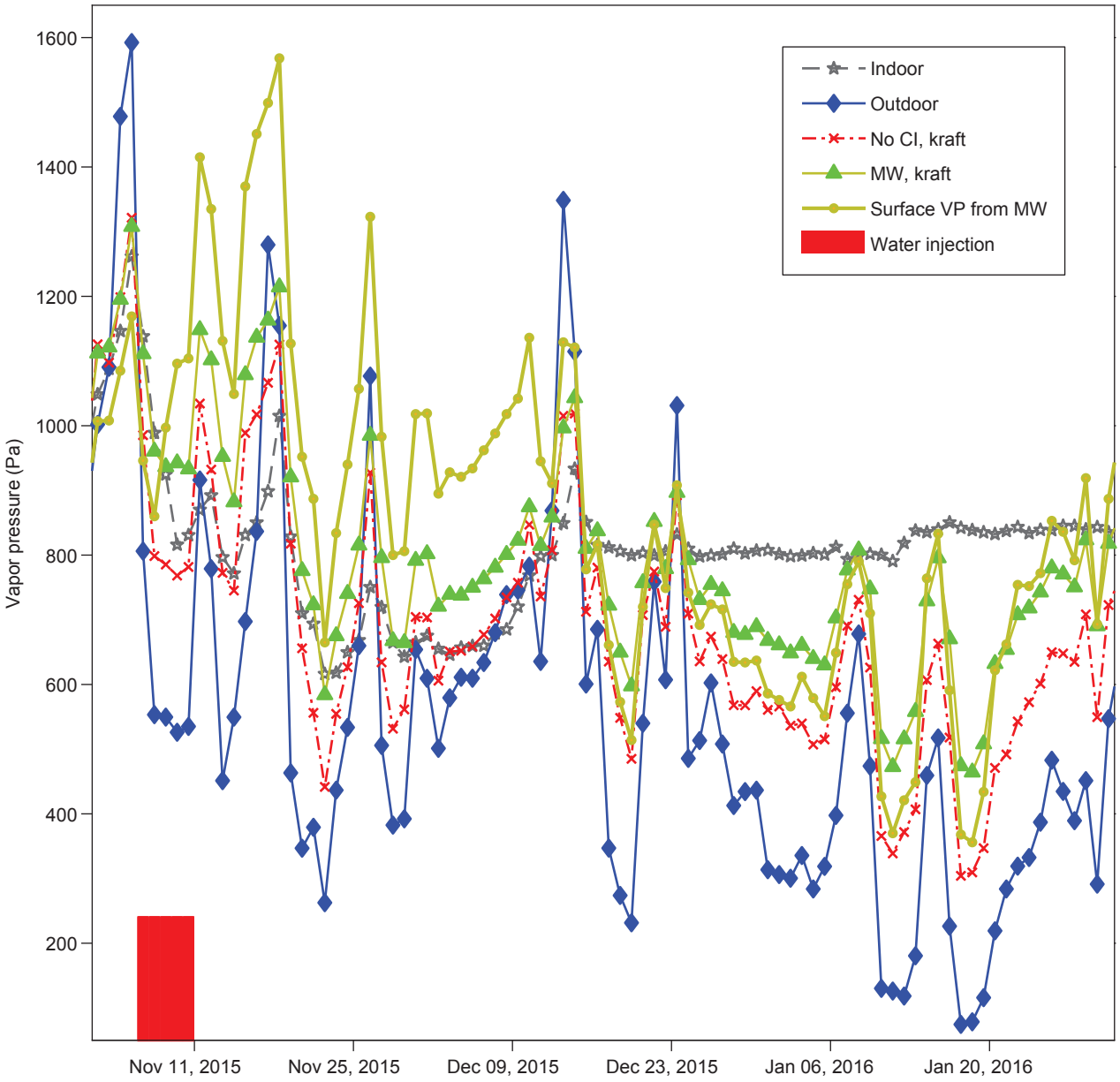


**Figure 23. Daily average vapor pressure after Injection 2 (CI, continuous insulation; MW, mineral wool; VP, vapor pressure).**

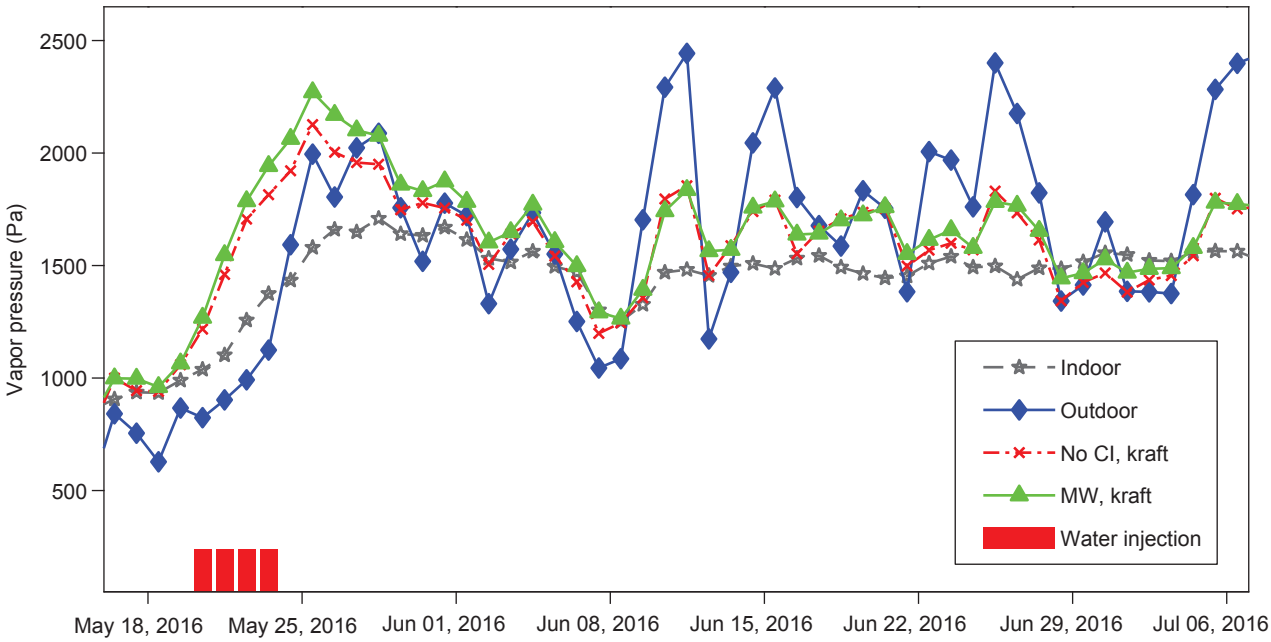


**Figure 24. Vapor pressures after Injection 3 (CI, continuous insulation; MW, mineral wool).**

## 3.4 Wood Moisture Contents

### 3.4.1 General Trends

The most basic trend in OSB MC was the rise in MC during the winter for the kraft-faced cavities caused by moisture diffusion from the interior humidification. This is illustrated by comparing weekly average MC values near the top plate for all the north walls in Figure 25. Only Walls 1 (no CI, kraft) and 8 (XPS, kraft, crinkled) were above 20% MC, and this was true only briefly during winter. During the winter, the kraft-faced cavities had higher MC than their corresponding cavities with polyethylene vapor retarders. The OSB near the top plate did not have a significant response to the water injections (shown as red bars in Figure 25).

In contrast to the OSB sheathing, the wood framing components did not exhibit a seasonal trend in MC but were slightly affected by the water injections, which is shown in the graphs again as a red bar indicating the timing of the injections. Figure 26 plots MC values in the 38- by 140-mm studs near midheight.

Figure 27 shows a larger effect from the water injections plotting the MC values in the field of the shop towel wetting system.

These same two effects can also be seen in the RH of the cavities. Figure 28 plots RH8, the HOBO sensor in midcavity, for Walls 3 (MW, draft) and 4 (MW, poly) showing the generally lower RH of Wall 4 (poly), but also the spikes caused by water injection, which can increase the RH of Wall 4 above Wall 3 until it dries out again. Further water injection results and drying potential will be presented in the following section.

Similar trends occurred in the south walls. Figure 29 illustrates this by comparing MC values in OSB at top of Wall 1 (no CI, kraft) for both north and south. Again in kraft-faced cavities such as Wall 1, there was significant moisture accumulation in the winter, higher in the first winter during which the indoor humidity set point was higher. The higher MC of the north walls might be expected because of the slightly higher temperature of the south walls (as a result of solar radiation), but this effect was small and not consistent in all results. More consistent was the result that walls with exterior insulation had lower MC than the base walls. Figure 30 illustrates this for all walls with polyethylene vapor retarders again plotting MC values near the top of the OSB. Figure 31 plots the MC of all south walls near the top of the OSB.

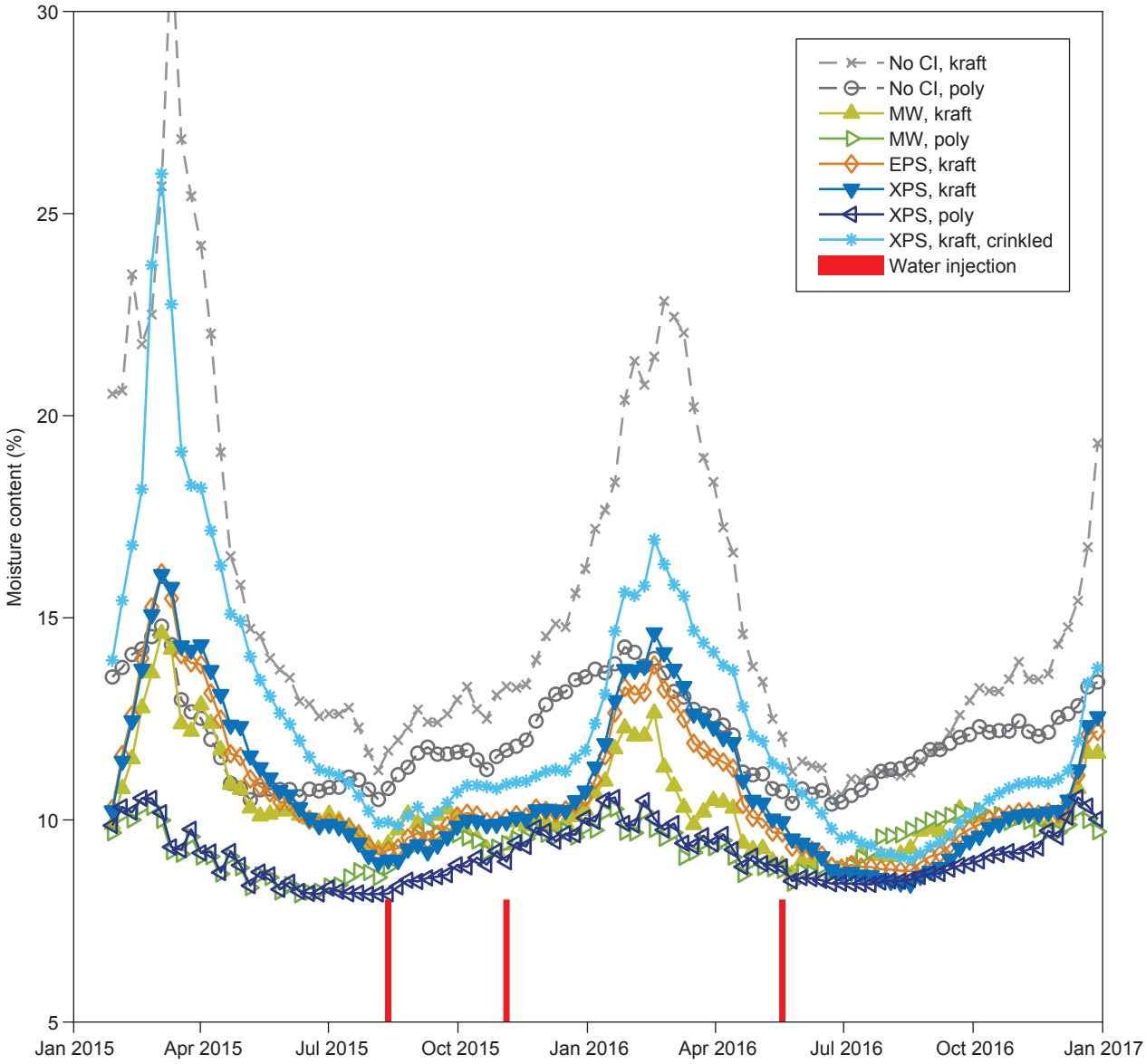


**Figure 25. Moisture content in oriented strandboard near top in north walls (CI, continuous insulation; MW, mineral wool; EPS, expanded polystyrene; XPS, extruded polystyrene).**

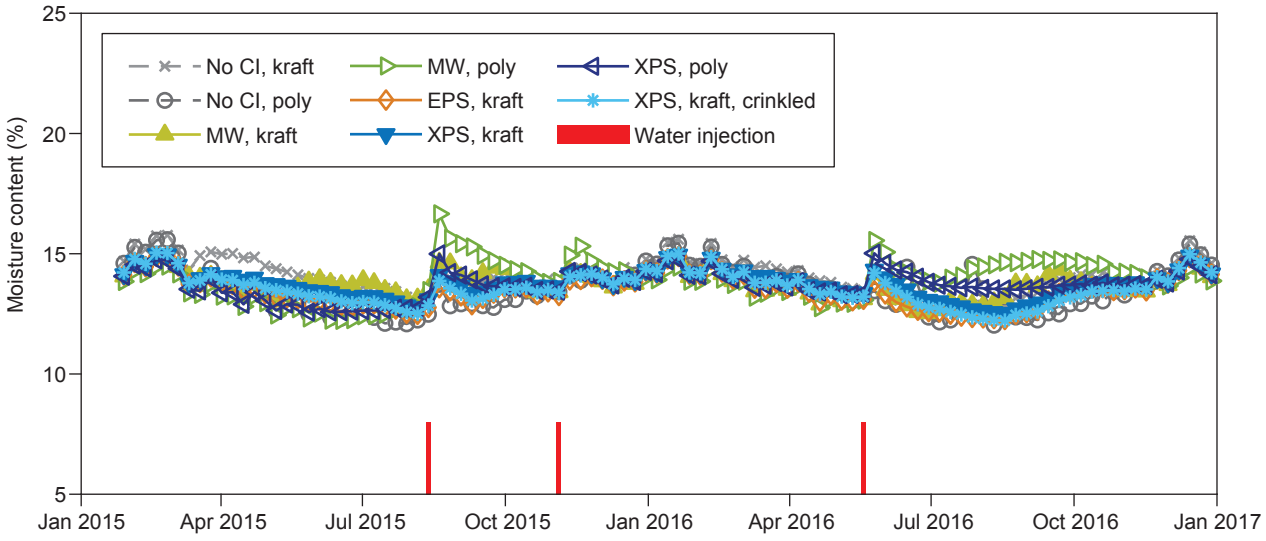


**Figure 26. Moisture content in studs at midheight in north walls (CI, continuous insulation; MW, mineral wool; EPS, expanded polystyrene; XPS, extruded polystyrene).**

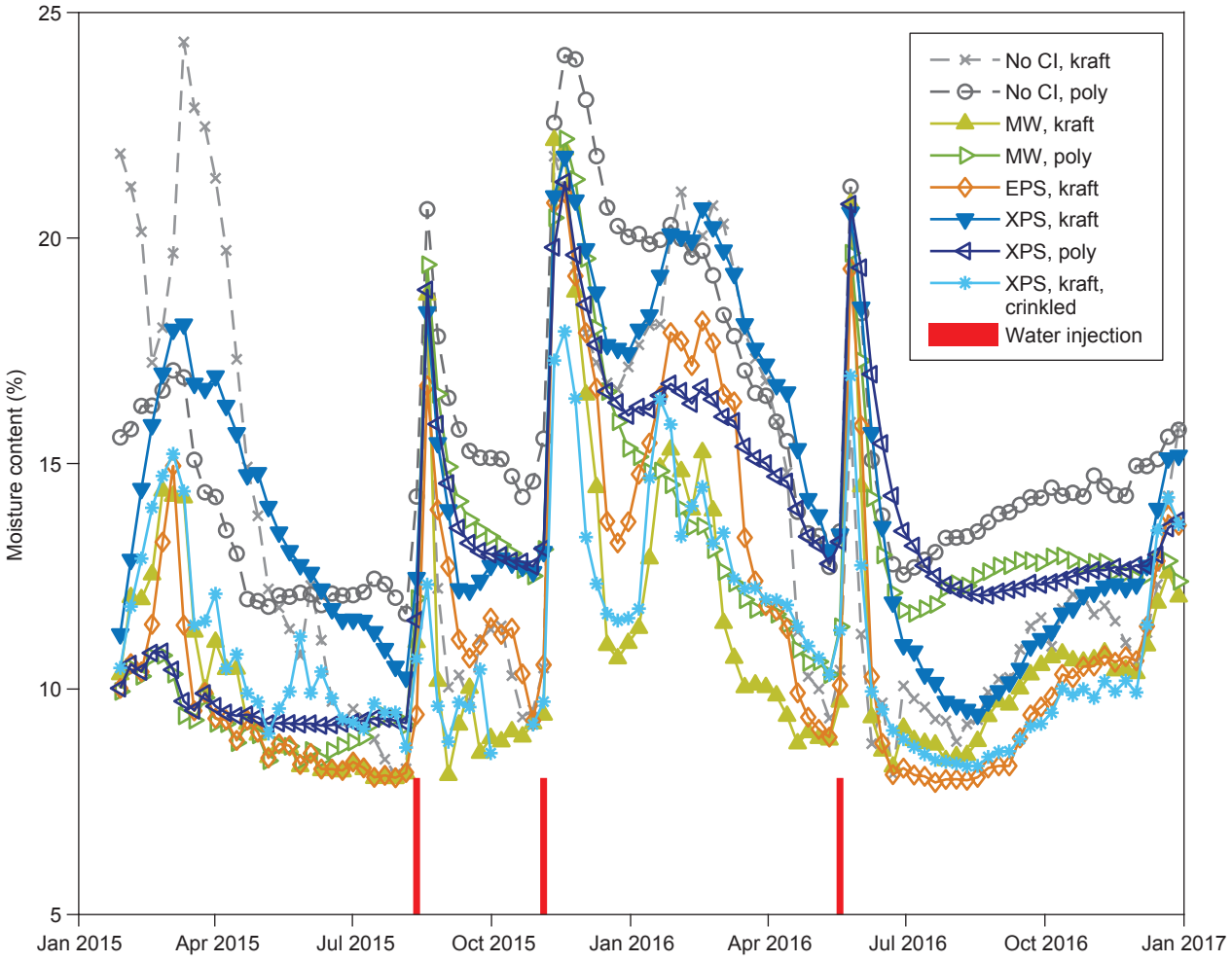


**Figure 27. Moisture content at water injection site in north walls (CI, continuous insulation; MW, mineral wool; EPS, expanded polystyrene; XPS, extruded polystyrene).**

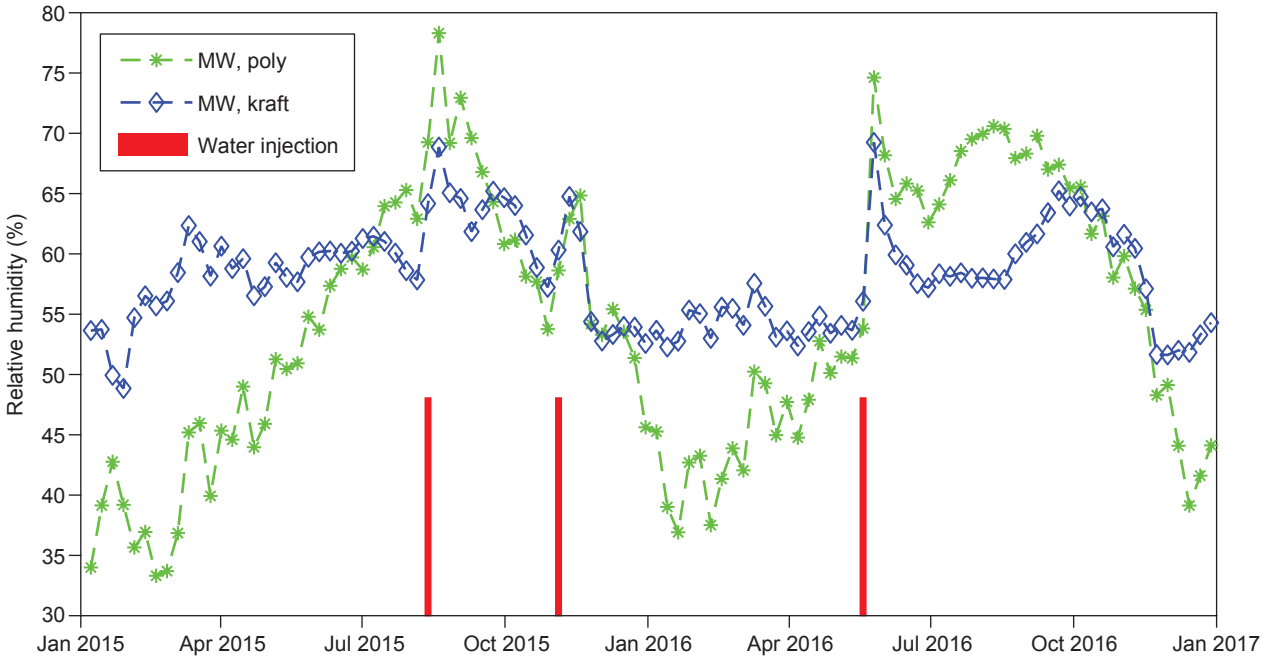


**Figure 28. Relative humidity from mineral wool (MW) walls, kraft and poly, with effects of water injection.**

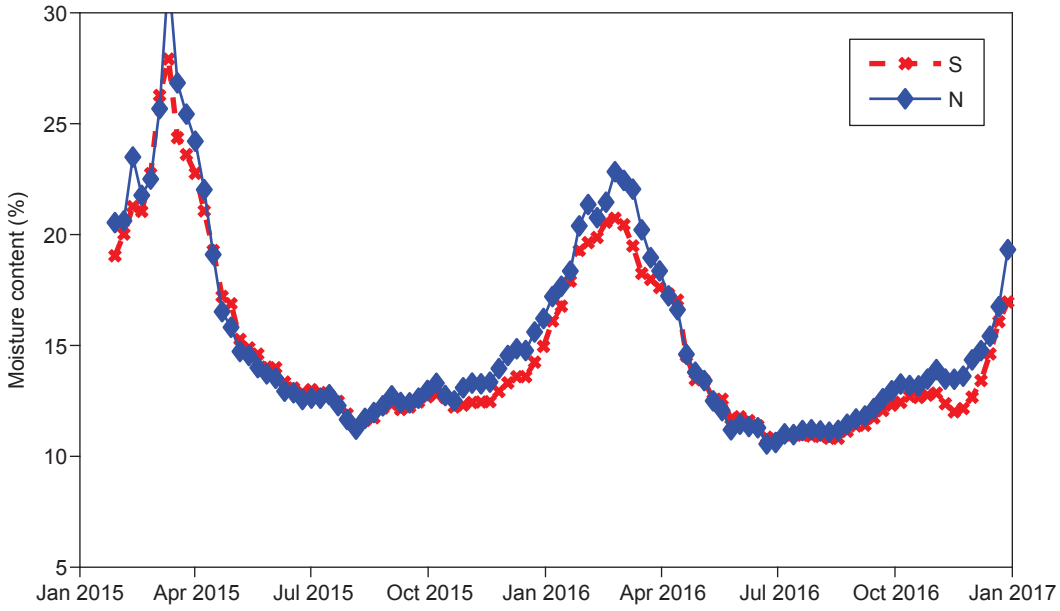


**Figure 29. Moisture content in oriented strandboard near top in no continuous insulation, kraft wall comparing north (N) and south (S) elevations.**

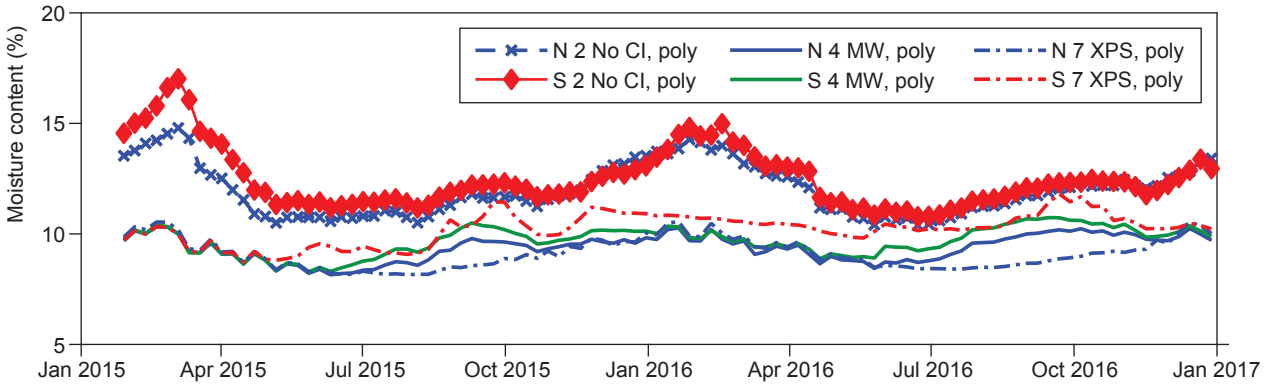


**Figure 30. Moisture content in oriented strandboard near top for all walls with polyethylene vapor retarder (CI, continuous insulation; MW, mineral wool; XPS, extruded polystyrene).**

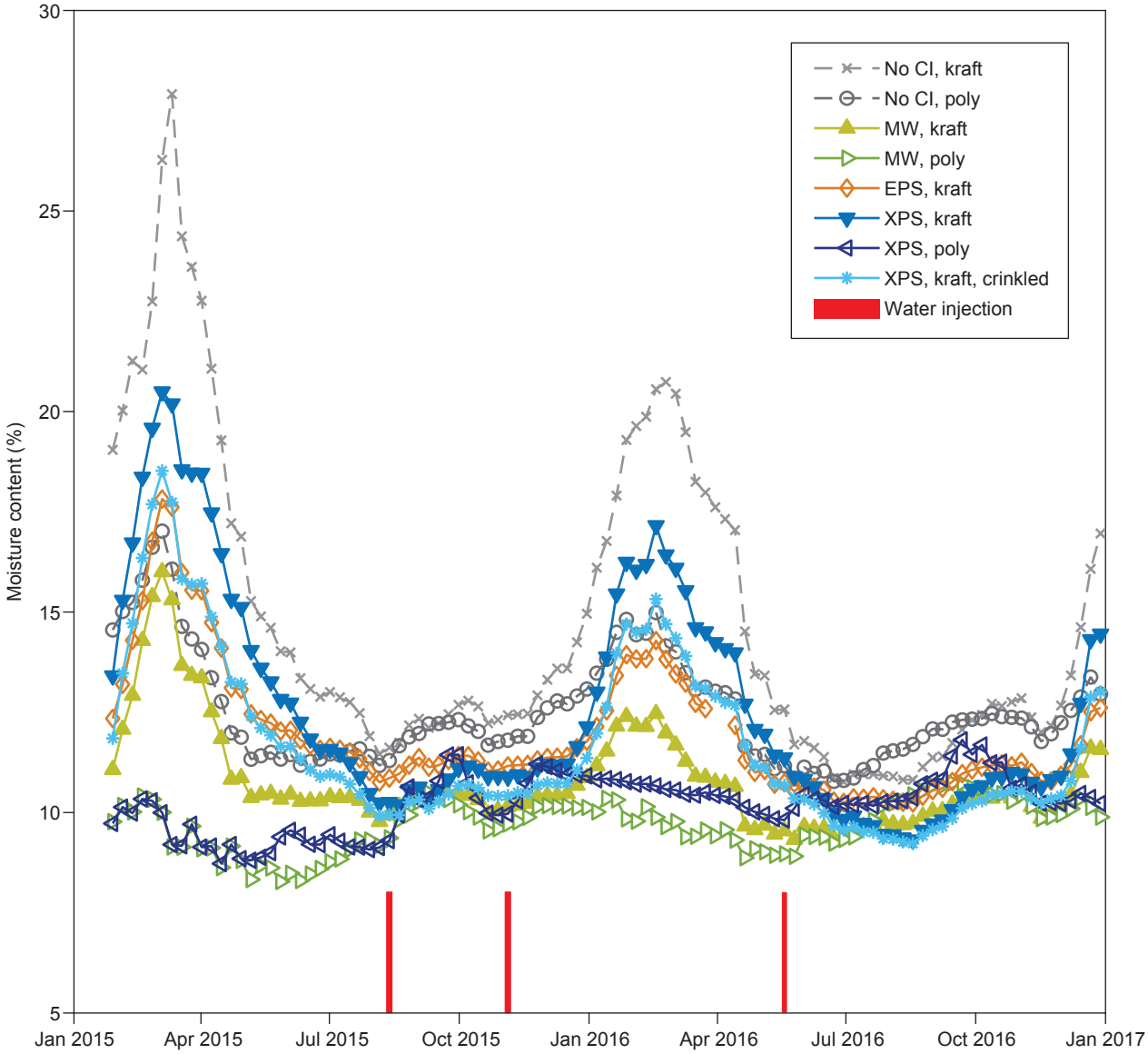


**Figure 31. Moisture content in oriented strandboard near top in south walls (CI, continuous insulation; MW, mineral wool; EPS, expanded polystyrene; XPS, extruded polystyrene).**

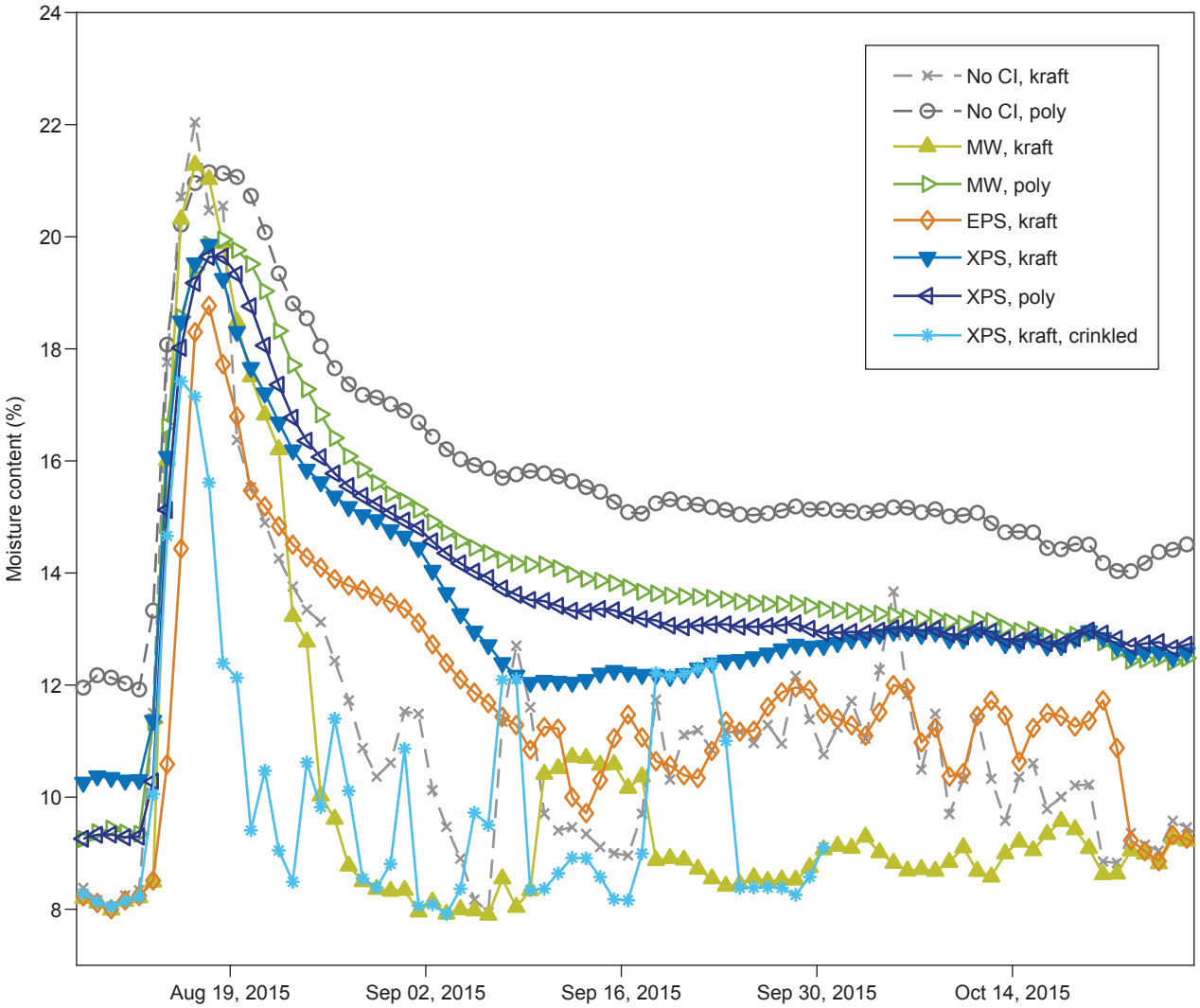


**Figure 32. Moisture content in oriented strandboard in field of wetting: daily averages around Injection 1 (Aug. 2015) for north walls (CI, continuous insulation; MW, mineral wool; EPS, expanded polystyrene; XPS, extruded polystyrene).**

### 3.4.2 Water Injection and Drying Potential

So far, results have been presented primarily as weekly averages, but for the discussion of drying after water injection, daily averages will be plotted around the times of the injection. Figure 32 presents the first drying period showing MC values in OSB in the field of the wetting for all north walls, whereas Figure 33 shows the same MC values for the south walls. In both cases, the kraft-faced cavities dried faster because they could dry inward.

The second and third drying periods are similar and will be discussed in more detail subsequently. Before reviewing these drying data, two other effects are illustrated in Figures 34 and 35, which plot the MC values near the bottom plate (near but outside the field of injection) during and after the second injection. This moisture pin (MC3) is not in the field of the paper towel and hence does not see the strong spike from water injection, but it does show both the lateral movement of water away from the field of the paper towel and the winter moisture accumulation in the OSB from the kraft vapor retarder. The modest rise in moisture from MC3 for all north walls on November 11 in Figure 34 is water migrating away from the shop towel. The rise in moisture from MC3 for some walls starting in January 2016 is the winter accumulation caused by indoor humidity.

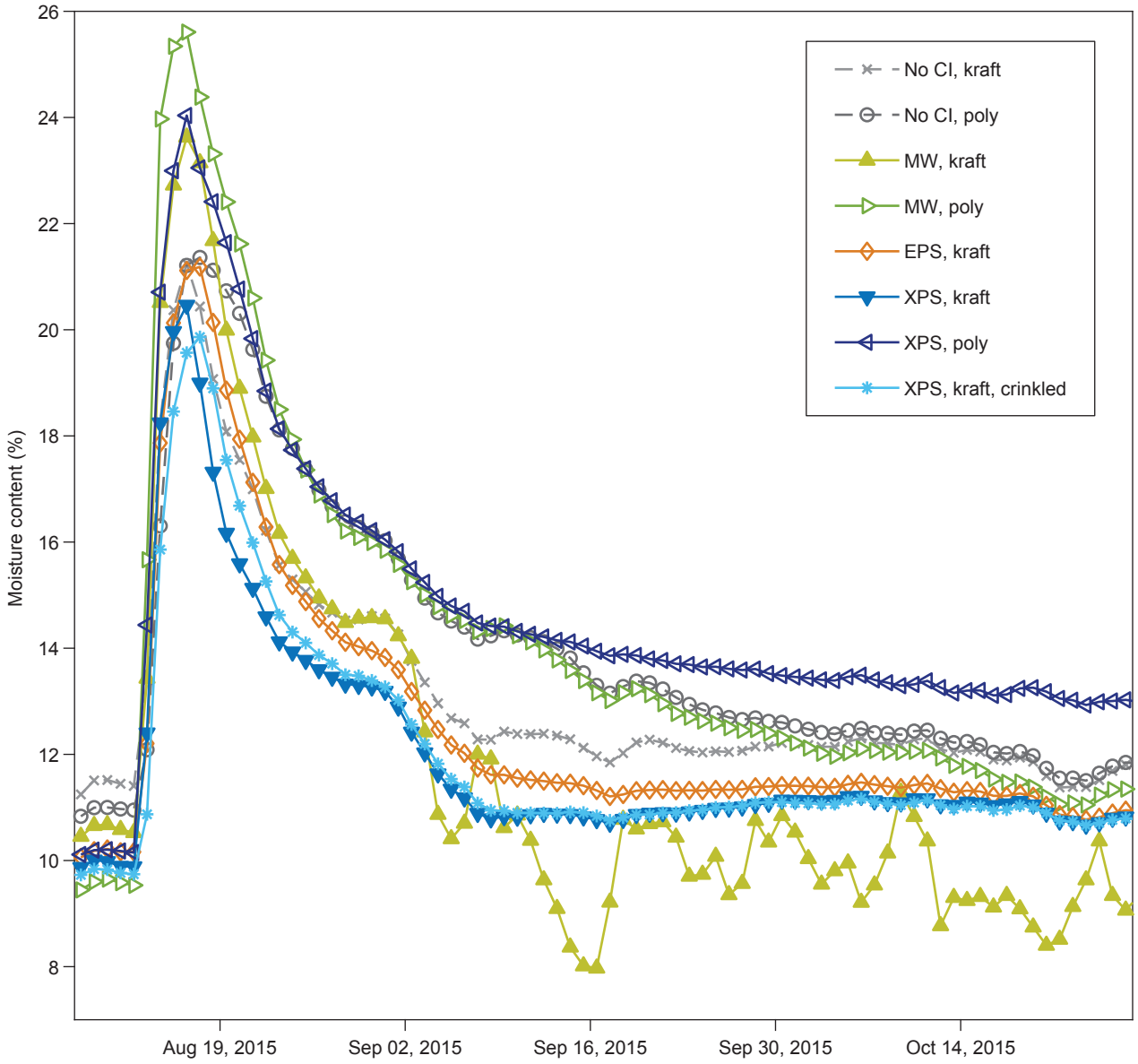


**Figure 33. Moisture content of oriented strandboard in field of wetting: daily averages around Injection 1 (Aug. 2015) for south walls (CI, continuous insulation; MW, mineral wool; EPS, expanded polystyrene; XPS, extruded polystyrene).**

Further analysis of drying will use a value, labeled $M5_{net}$, which normalizes all the MC5 values (in the field of wetting system) by subtracting the value of MC on August 8, 2015, in each wall from all the other values of MC for that wall. This forces each wall to start at an $M5_{net}$ value of zero just before the first injection thus allowing easy comparison of the changes in MC across walls. In addition, the focus will be primarily on the walls with polyethylene, which forces outward drying only. Figures 36 and 37 present $M5_{net}$ for the first injection for north and south walls, respectively. Figures 38 and 39 are the same for the second injection, and Figures 40 and 41 show the third injection.

A number of observations can be confirmed by inspection of Figures 36 through 41. First, the walls had not completed drying before the second injection in late fall of 2015. Second, all walls except those with XPS had returned to near initial conditions before the third injection. Third, in the winter, the walls with MW were able to dry quickly.

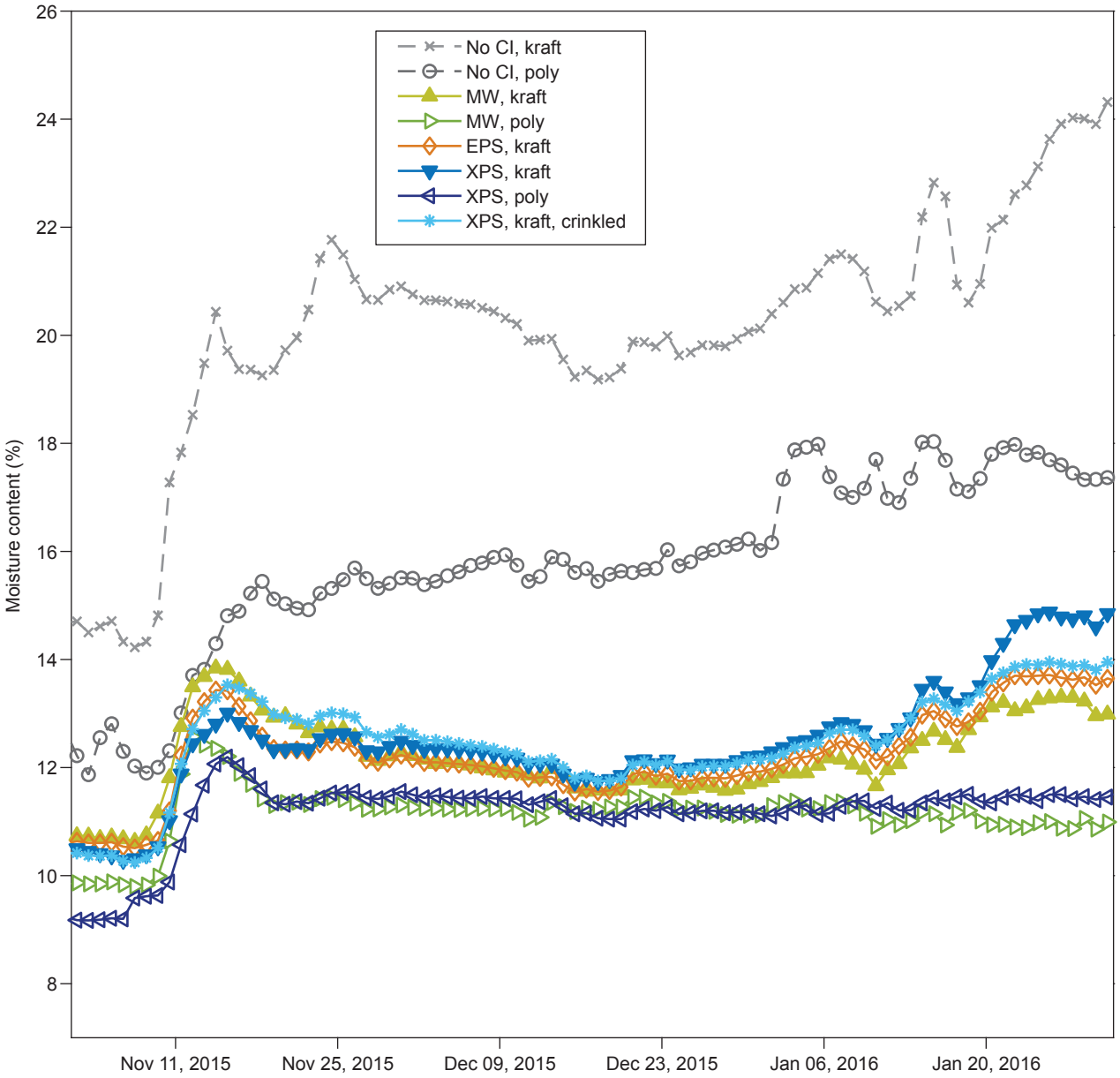


**Figure 34. Moisture content in oriented strandboard near bottom plate: daily averages around Injection 2 (Nov. 2015) for north walls (CI, continuous insulation; MW, mineral wool; EPS, expanded polystyrene; XPS, extruded polystyrene).**

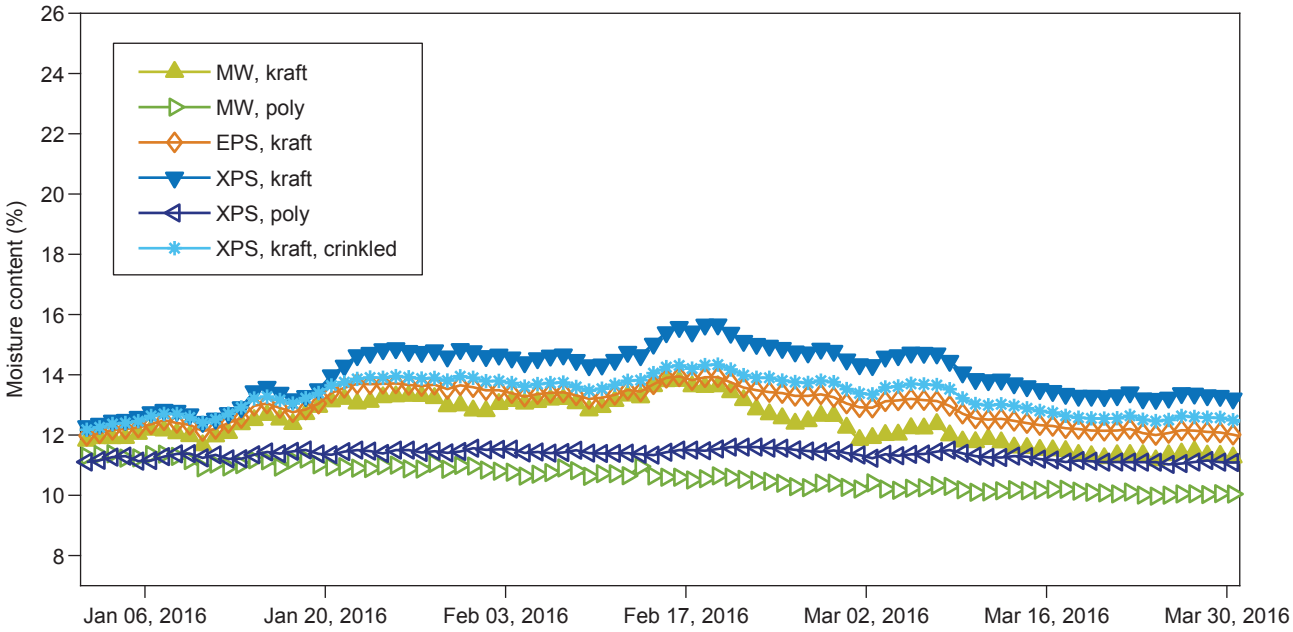


**Figure 35. Moisture content in oriented strandboard near bottom plate: daily averages during second winter for north walls (MW, mineral wool; EPS, expanded polystyrene; XPS, extruded polystyrene).**

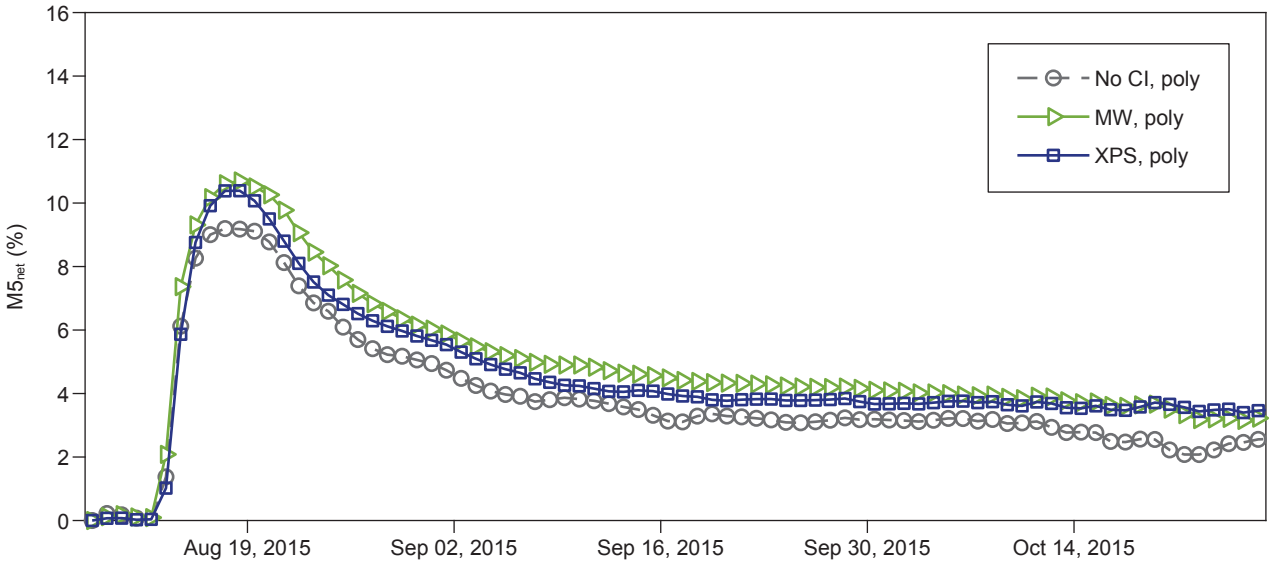


**Figure 36. Net moisture content around the time of Injection 1 (Aug. 2015) for north walls (CI, continuous insulation; MW, mineral wool; XPS, extruded polystyrene).**

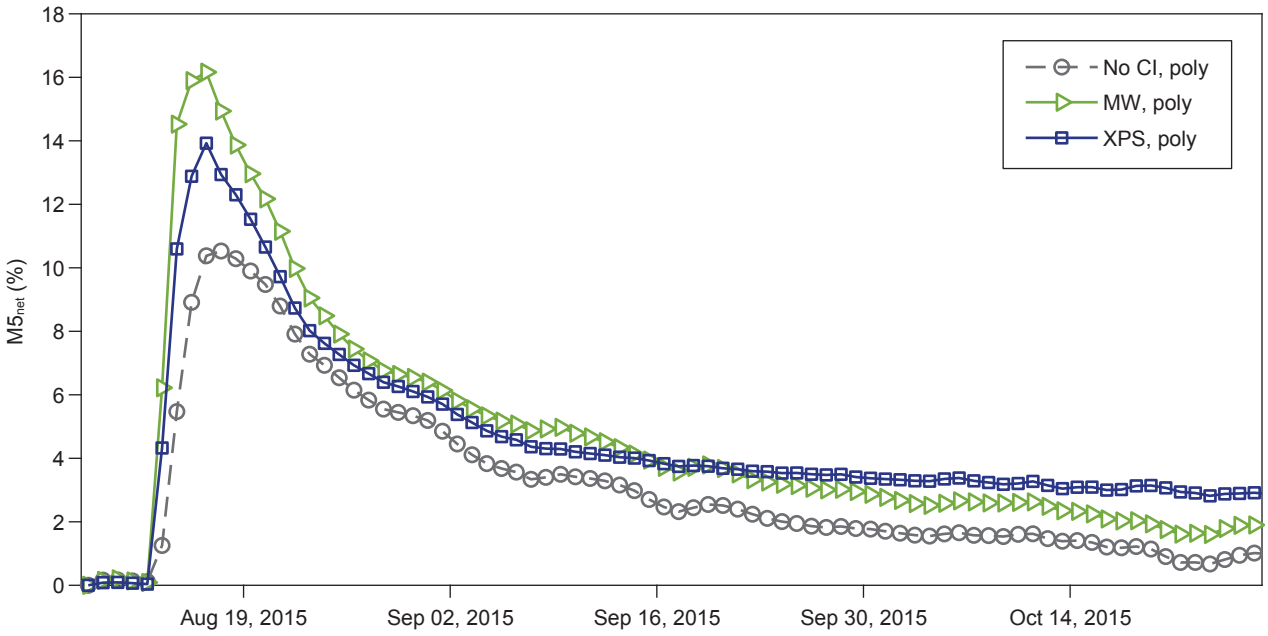


**Figure 37. Net moisture content around the time of Injection 1 (Aug. 2015) for south walls (CI, continuous insulation; MW, mineral wool; XPS, extruded polystyrene).**

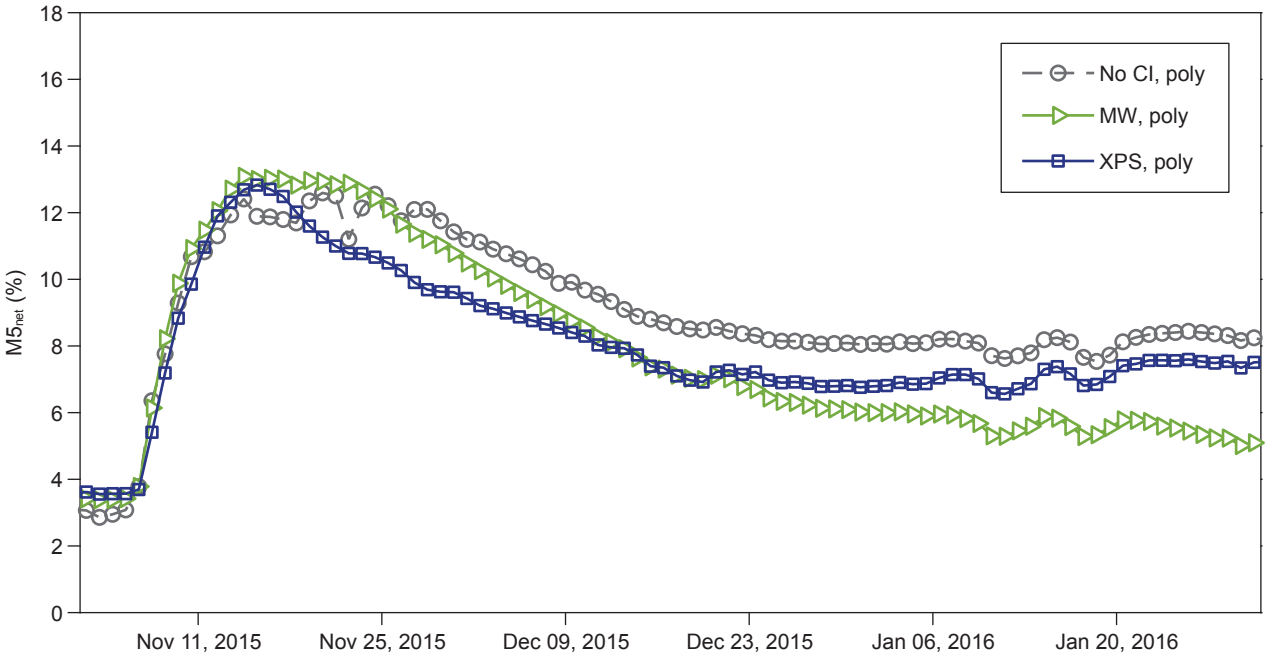


**Figure 38. Net moisture content around the time of Injection 2 (Nov. 2015) for north walls (CI, continuous insulation; MW, mineral wool; XPS, extruded polystyrene).**

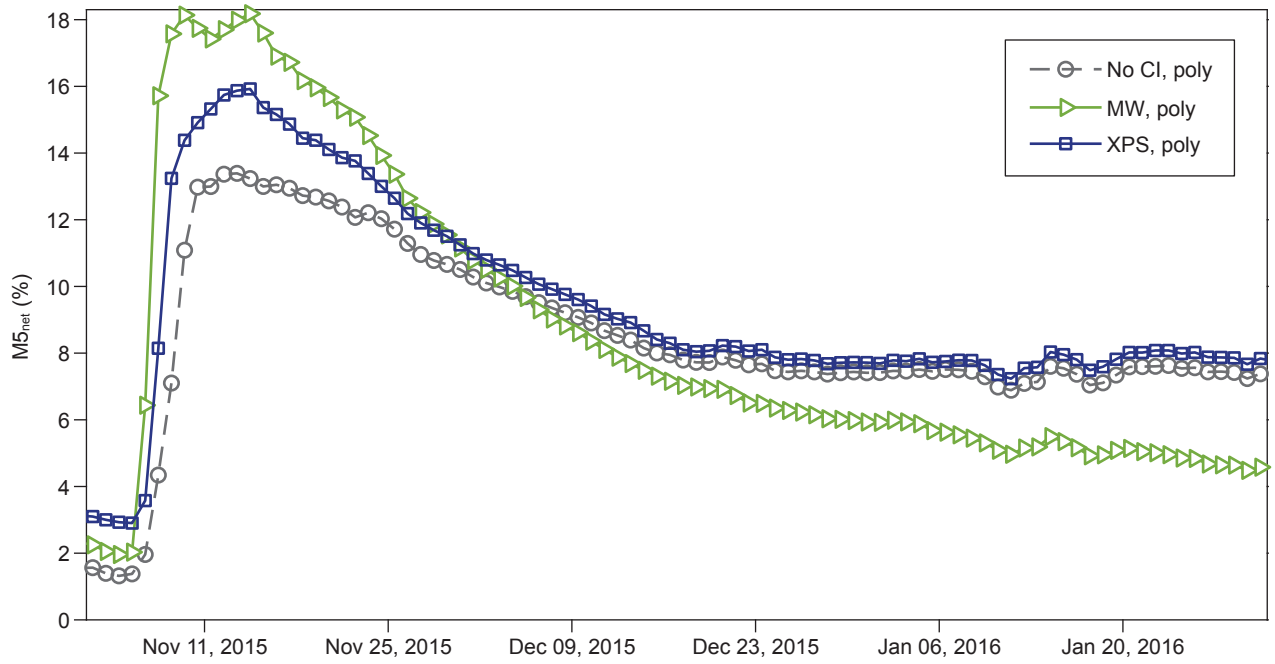


**Figure 39. Net moisture content around time of Injection 2 (Nov. 2015) for south walls (CI, continuous insulation; MW, mineral wool; XPS, extruded polystyrene).**

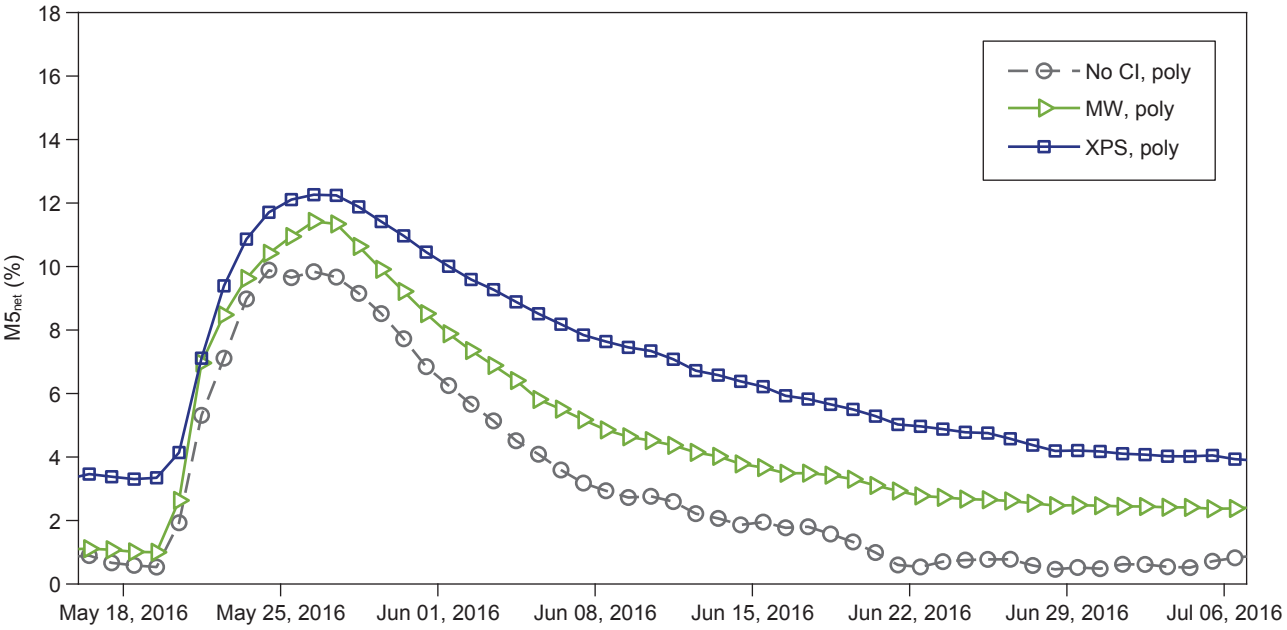


**Figure 40. Net moisture content around time of Injection 3 (May 2016) for north walls (CI, continuous insulation; MW, mineral wool; XPS, extruded polystyrene).**

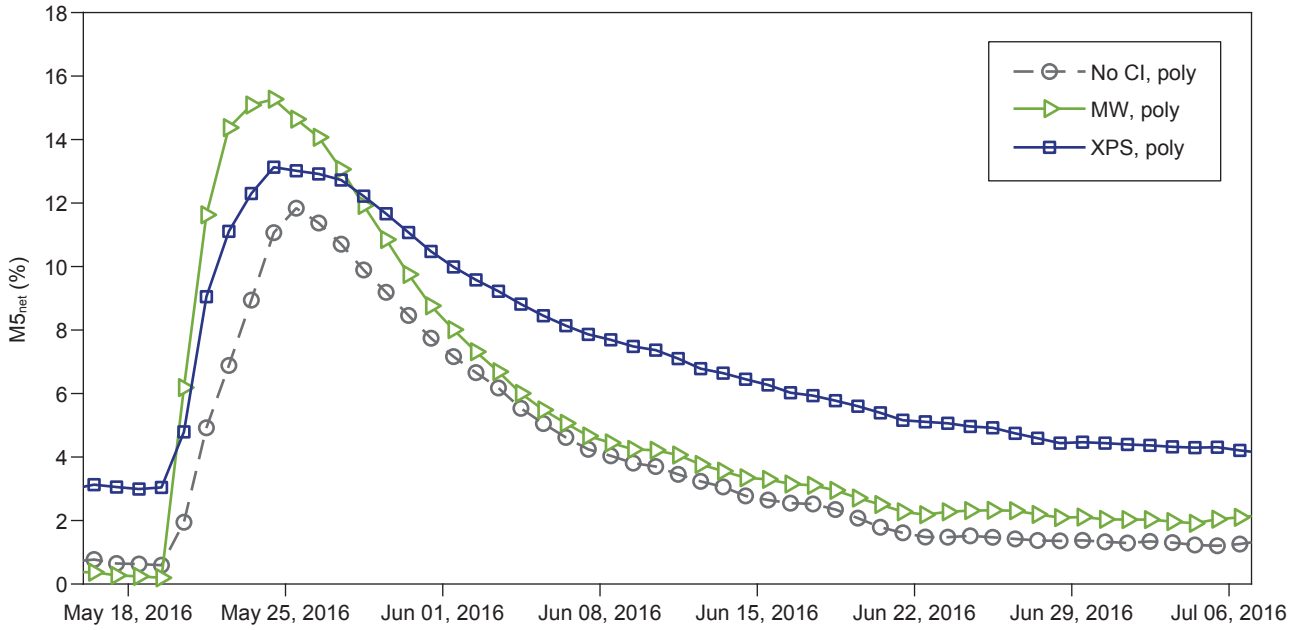


**Figure 41. Net moisture content around the time of Injection 3 (May 2016) for south walls (CI, continuous insulation; MW, mineral wool; XPS, extruded polystyrene).**

### 3.4.3 Quantification of Drying Potential

To quantify the drying behavior, each series of MC data in Figures 36 through 41 was fit with a near-exponential decay curve with a variable scale factor ($K$):

$$f(t) = K\left(\frac{1}{1+t\left(\frac{c}{\tau}\right)}\right)^{\frac{1}{c}} \qquad (2)$$

Details of the fit method are provided in Appendix B, whereas the basic near-exponential decay function is detailed in Whitehead and others (2009). A smaller time constant (τ) indicates more rapid drying, but the shape of the curve is also influenced by $c$, which controls the deviation from pure exponential decay. To compare how τ varies for all walls, $c$ was fixed at 0.756 and τ was plotted in the bar graph of Figure 42.

Overall, drying was faster during winter for walls with interior kraft paper compared with those with polyethylene, and the MW exterior insulation showed faster drying during the winter than the base walls and walls with other exterior insulation materials.

Further comparison will focus first on the walls with polyethylene, which only dried outward. The same decay function was fit but $c$ was allowed to rise to 1.33, which reflects slower drying. $T$ is compared for these walls in Table 4.

Again, the MW walls improved drying potential during winter. Very similar trends can also be seen in the kraft-faced walls. Applying the decay function fit yields a $c$ of 0.372, reflecting the faster response possible because of drying in both directions. The associated τ values for these kraft-faced walls are shown in Table 5.

Finally, the same trends can also be seen using a simpler measure of drying potential. Table 6 shows the percentage of the initial maximum net MC still left in each polyethylene wall 5 weeks after the injections stopped. Again, smaller numbers indicate faster drying. Only the polyethylene walls are reported in Table 6, similar to Table 4.

**Table 4—Drying time constants (days) for walls with interior polyethylene vapor retarders[a]**

| Injection | Wall | No CI | MW | XPS |
|---|---|---|---|---|
| 1, Aug–Sept | N | 17 | 24 | 23 |
| 1, Aug–Sept | S | 7 | 7 | 11 |
| 2, Nov–Dec | N | 103 | 35 | 70 |
| 2, Nov–Dec | S | 64 | 19 | 52 |
| 3, May–June | N | 5 | 10 | 14 |
| 3, May–June | S | 5 | 6 | 15 |

[a]N, north; S, south; CI, continuous insulation; MW, mineral wool; XPS, extruded polystyrene.

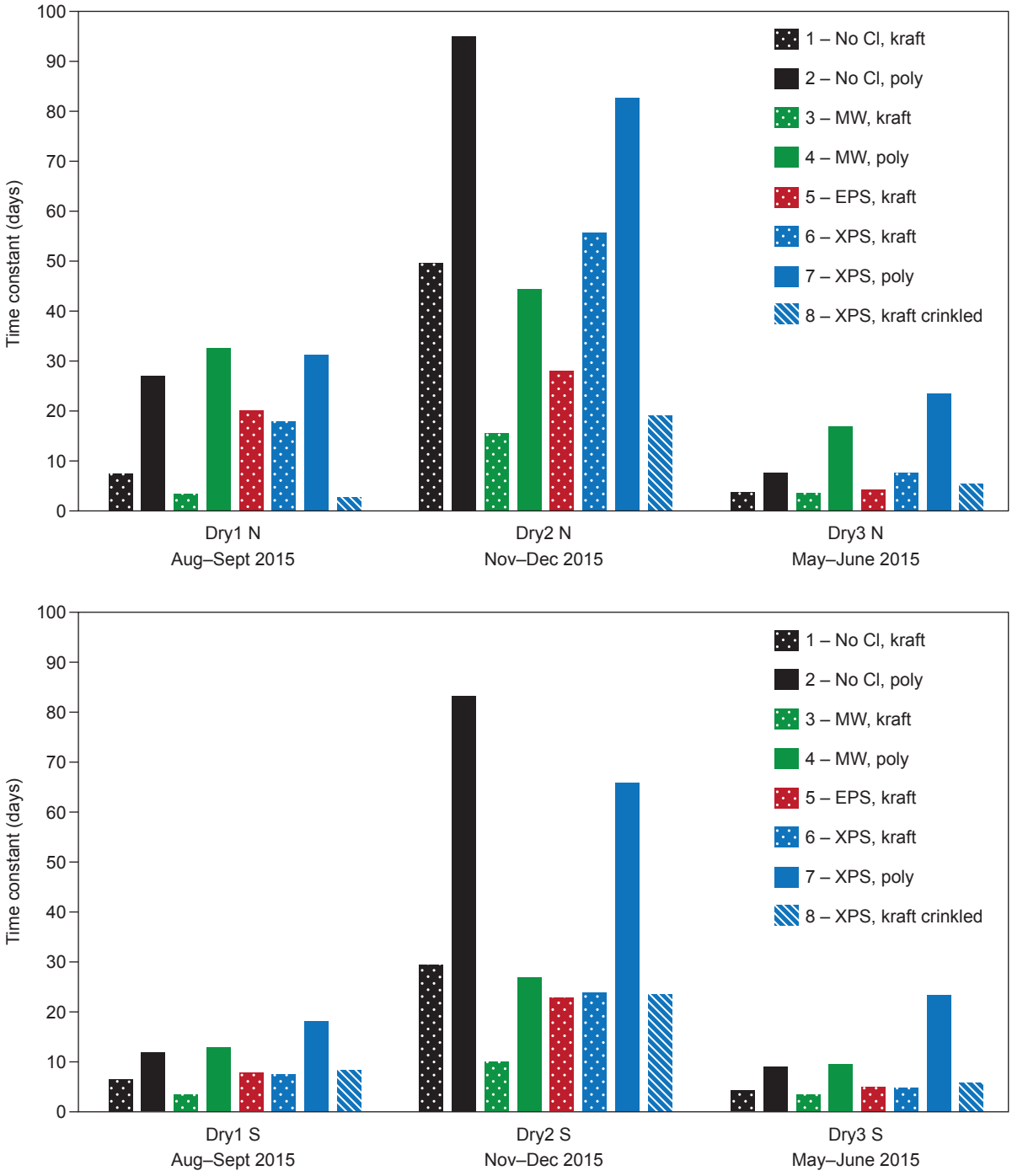


**Figure 42. Drying time constants for all walls (CI, continuous insulation; MW, mineral wool; EPS, expanded polystyrene; XPS, extruded polystyrene).**

**Table 5—Drying constants (days) for kraft-faced walls[a]**

| Injection | Wall | No CI | MW | EPS | XPS | XPS-cr |
|---|---|---|---|---|---|---|
| 1, Aug–Sept | N | 10 | 4 | 26 | 23 | 4 |
| 1, Aug–Sept | S | 10 | 5 | 11 | 11 | 12 |
| 2, Nov–Dec | N | 55 | 19 | 33 | 62 | 22 |
| 2, Nov–Dec | S | 34 | 13 | 29 | 29 | 28 |
| 3, May–June | N | 5 | 5 | 6 | 10 | 7 |
| 3, May–June | S | 6 | 4 | 7 | 7 | 9 |

[a]N, north; S, south; CI, continuous insulation; MW, mineral wool; EPS, expanded polystyrene; XPS, extruded polystyrene; XPS-cr, extruded polystyrene crinkled.

**Table 6—Percentage of initial peak net MC after 5 weeks drying in walls with polyethylene vapor retarders[a]**

| Injection | Wall | No CI | MW | XPS |
|---|---|---|---|---|
| 1, Aug–Sept | N | 35 | 41 | 38 |
| 1, Aug–Sept | S | 22 | 23 | 28 |
| 2, Nov–Dec | N | 65 | 55 | 57 |
| 2, Nov–Dec | S | 58 | 39 | 54 |
| 3, May–June | N | 5 | 22 | 34 |
| 3, May–June | S | 12 | 14 | 34 |

[a]N, north; S, south; CI, continuous insulation; MW, mineral wool; XPS, extruded polystyrene.

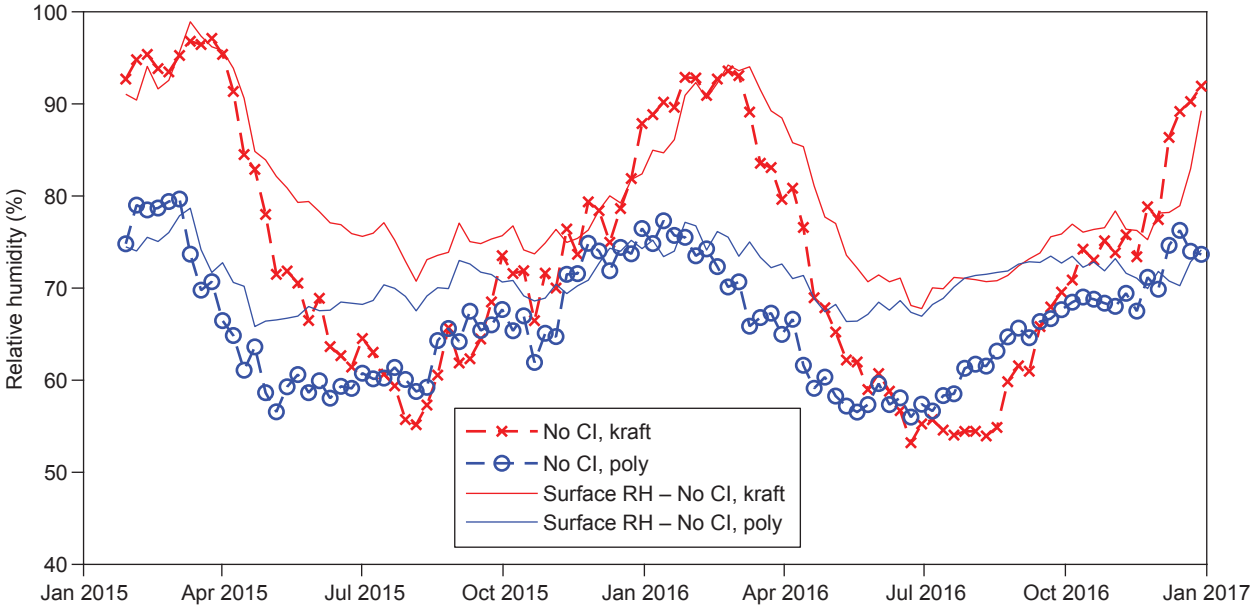


**Figure 43. Surface relative humidity (RH) compared with measured RH near top of base case north walls (CI, continuous insulation).**

## 3.5 OSB "Surface" Relative Humidity Levels

In this section, the OSB sorption isotherm detailed in Appendix A is again used to calculate apparent surface RH. Note that the moisture pins extended through the depth of the OSB, recording the lowest resistance path at any depth, and hence may not always represent the surface RH but instead the highest RH in the OSB. Here we present the apparent surface RH calculated from MC1 in OSB near the top of each wall. Figure 43 plots that surface RH along with the measured RH near that location for the two north base walls.

Generally, the surface RH tracked the measured cavity RH but did not drop as much during the summer, and clearly kraft-faced walls had higher RH than walls with polyethylene barriers during winter. The expected result that kraft-faced walls had higher RH during winter is also illustrated in Figure 44, which plots surface RH for all north walls. In addition, inspection of Figure 44 shows that adding exterior insulation lowers surface RH.

That effect can be seen again in Figure 45, which compares the differences between north and south walls for the base case and the MW case. Furthermore, the south walls sometimes had slightly higher surface RH.

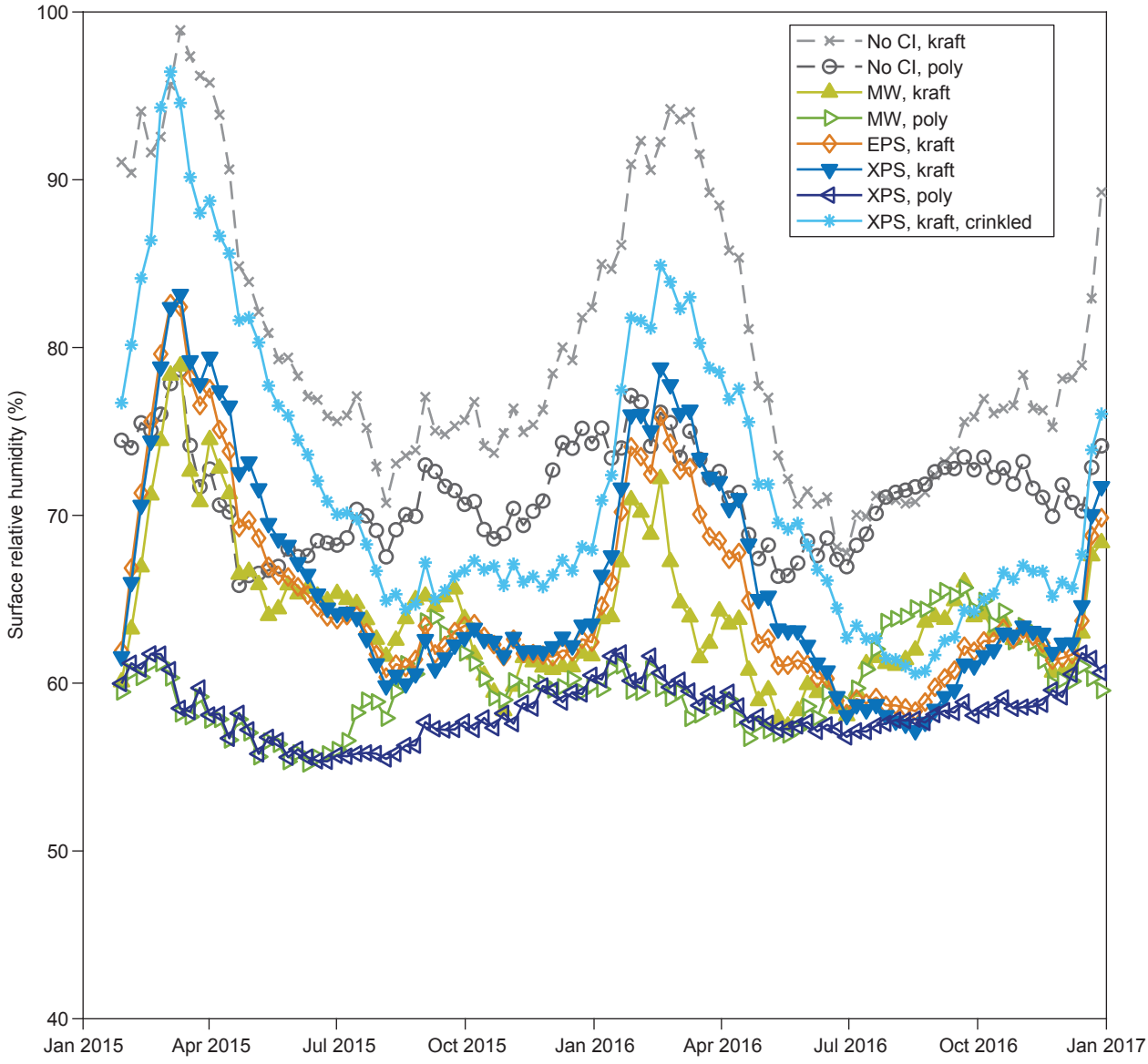


**Figure 44. Surface relative humidity for all north walls (CI, continuous insulation; MW, mineral wool; EPS, expanded polystyrene; XPS, extruded polystyrene).**

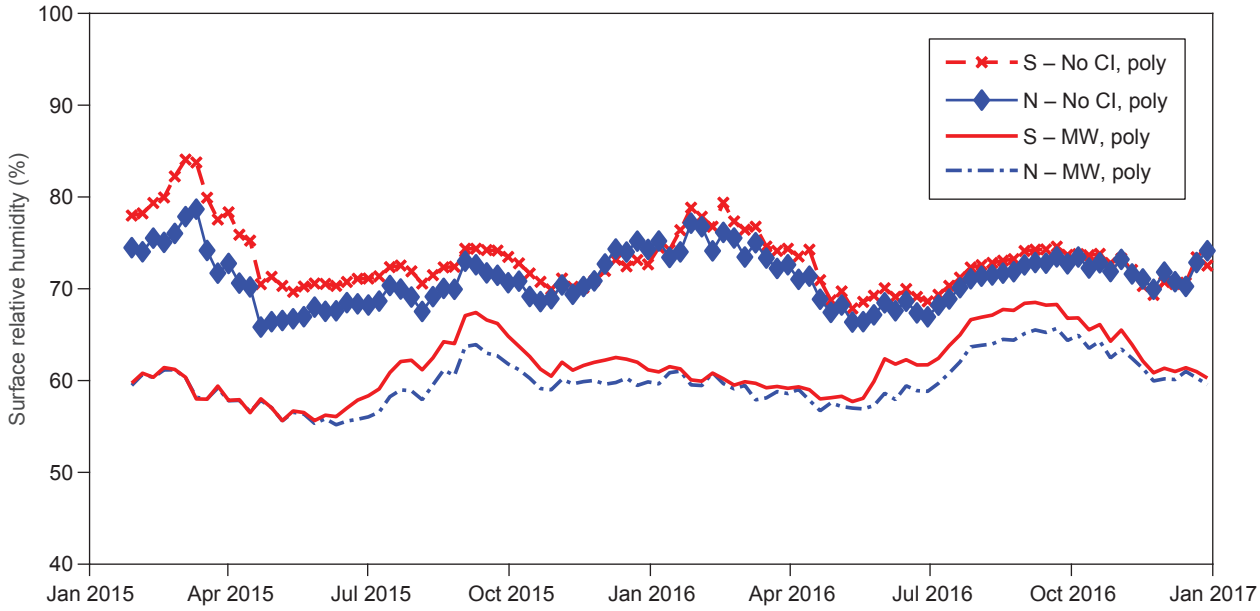


**Figure 45. Surface relative humidity north (N) compared with south (S) for base and mineral wool (MW) walls (CI, continuous insulation).**

# 4 Discussion

Moisture accumulation was observed in OSB sheathing during winter to the largest extent in Walls 1N and 1S with no exterior insulation and interior kraft vapor retarder. Moisture contents were above 20% in both winters; they reached higher levels in the first winter than in the second winter as a result of the higher interior humidity conditions. These walls dried rapidly in springtime. Sherwood (1983) and Parsons and others (2016) also measured wintertime sheathing MC above 20% in 38- by 140-mm walls with kraft vapor retarders and no exterior insulation, although Rose and McCaa (1998) measured considerably lower peak MC in similar wall assemblies.

Traditional guidance for protection of wood from decay has been to keep the MC below 20% (Carll and Highley 1999). In this case, the risk of wood decay was probably quite low because the periods of high MC coincided with cold temperatures and the walls dried rapidly in warmer weather. The risk of mold growth on OSB, which depended on the surface temperature and moisture conditions, will be addressed in a separate report.

In the remaining wall assemblies, the OSB MC remained in a safe range during the 2-year investigation despite being challenged by high interior humidity in winter. It was expected that the walls with kraft vapor retarders and exterior insulation would have lower wintertime OSB MC than the corresponding walls without exterior insulation as a result of the exterior insulation warming the OSB sheathing.

All wall assemblies were able to accommodate controlled wettings multiple times during the study. The water injections were not severe but were enough to stress the wall around the injection site, similar to a localized water leak. The "drying" that occurred in $M5_{net}$ after injections was a combination of water redistribution away from the moisture pin and water leaving the OSB. The moisture pin data alone cannot help us determine the proportion between redistribution and actual drying. Further research is underway to help understand the effect of redistribution on MC readings. The observed decrease in OSB MC after controlled wetting events depended on weather conditions, type of exterior insulation, and type of interior vapor retarder. The temperature of the OSB had a large effect on the drying rate (i.e., rate of decrease in M5 in the field of the wetting towel). In all walls, the drying rate was much slower during the cold months. During warm periods, the XPS exterior insulation slowed down but did not prevent outward drying. However, during winter, the XPS exterior insulation sped up drying somewhat relative to the case without exterior insulation because the OSB was warmer. This effect was more dramatic in the vapor-open MW, which significantly improved drying during winter. The faster drying of walls with vapor-open MW than comparable walls with XPS is consistent with prior work by Maref and others (2011), Fox and others (2014), and Trainor and others (2016). Given that both MW and XPS warm the OSB during winter and redistribution would be expected to be similar, some water must be actually leaving the OSB because the wall with MW dried more quickly than the wall with XPS. In addition, walls with kraft vapor retarders generally dried more quickly than corresponding walls with polyethylene.

# 5 Conclusions

The results of this study support the conclusion that adding exterior insulation does not increase the risk of moisture-related deterioration in wood-framed wall assemblies. For 2 years, we monitored the performance of a wood-framed structure in a cold climate built with 38- by 140-mm lumber and 11-mm-thick OSB sheathing. We tested two interior vapor retarders (kraft-faced fiberglass cavity insulation and polyethylene sheeting) in combination with commonly used exterior insulation materials, including XPS, EPS, and MW. Adding 25.4 mm of XPS to a wall with an interior vapor barrier did not prevent the wall from drying under modest load. Although under some conditions, a low permeance exterior material does slow drying, exterior insulation also keeps the wall warmer during cold weather, thereby enhancing moisture movement. The drying benefit of exterior insulation during cold weather is enhanced by using vapor-permeable exterior insulation such as MW. Vapor-open exterior insulation allowed our test walls to dry more quickly during winter that our base walls insulated only with fiberglass in the cavity. We also found that the kraft facing of fiberglass insulation did not prevent moisture accumulation in the exterior OSB during winter. The magnitude of this effect depended on interior RH conditions. In very few cases did the OSB MC rise to dangerous levels, but concurrent low temperatures decreased decay potential and the walls always dried out quickly in the spring when warm weather arrived.

# Acknowledgments

This manuscript was improved by comments from Marshall Begel. The authors gratefully acknowledge the help of many FPL colleagues during the course of this investigation. Also, the support of APA – The Engineered Wood Association was instrumental in furthering this work. This work was funded by the USDA Forest Service, Forest Products Laboratory, and APA – The Engineered Wood Association through Joint Venture Agreement 14-JV-11111136-054.

# Appendix A—Apparent Surface Relative Humidity Calculations

When the apparent surface RH of OSB is calculated from an MC reading, either to compare with other RH measurements or to calculate vapor pressure, an OSB sorption isotherm is needed to relate RH and MC. There is a large range of values in the literature for OSB sorption isotherms. Further experimental work is warranted. For this report, we used the same sources documented in Boardman and others (2017), averaging the adsorption and desorption values to generate a generic OSB sorption curve suitable for quick calculation of RH given OSB MC. Because we had no temperature-dependence data for OSB, we used the temperature dependence of an existing correlation for wood discussed as "H4" in Glass and others (2014). We then fit that formula to our room temperature data for OSB, only optimizing the fit parameters that were not temperature related. The generic formula is given in Equation (A-1) with $m$ as the decimal MC (0–1), $h$ as the decimal RH (0–1), and $T$ as absolute temperature (K).

$$m = \left[ AT\left(1-\frac{T}{T_c}\right)^{B} \ln\left(1-h\right) \right]^{CT^{D}} \quad \text{(A-1)}$$

where $A$, $B$, $C$, and $D$ are fitting parameters and critical temperature $T_c$ = 647.1 K. Our fit was constrained to yield less error at the high RH region. The inverted formula to calculate $h$ given $m$ is shown with final values in Equation (A-2) and plotted in Figure 46.

$$h = 1-\exp\left[ \frac{-1520}{T}\left(1-\frac{T}{647.1}\right)^{-2.43} m^{17.3T^{-0.451}} \right] \quad \text{(A-2)}$$

The time response of the MC sensors is somewhat delayed relative to the surface RH, because any RH fluctuations are damped by the storage capacity of the OSB sheathing. Furthermore, the moisture pins read the highest MC anywhere throughout the depth of the OSB. For these reasons, we refer to calculated values as "apparent" surface RH values.

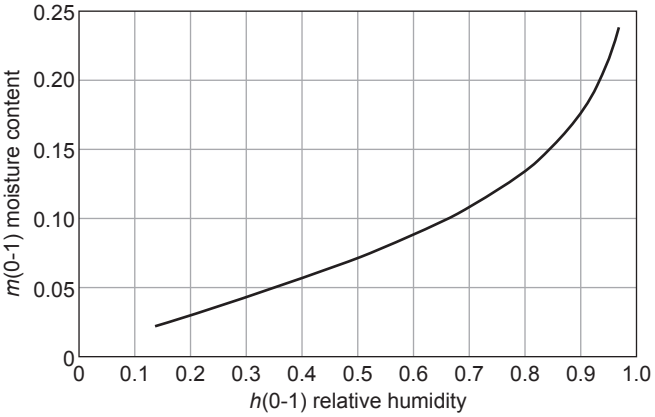


**Figure 46. Oriented strandboard sorption isotherm at 23 °C.**

# Appendix B—Moisture Content Decay Function

To help quantify the drying behavior of the OSB walls, the $M5_{net}$ values were fit to a near-exponential decay function. Background and details on the function can be found in Whitehead and others (2009). The equation is presented in Equation (B-1) and plotted in Figure 47 with a scale factor ($K$) of 12.

$$f(t) = K\left(\frac{1}{1+t\left(\frac{c}{\tau}\right)}\right)^{\frac{1}{c}} \qquad \text{(B-1)}$$

where $t$ is time (days), $c$ is a dimensionless shape parameter, and $\tau$ is a decay time constant (days). The $c$ value, which must be greater than 0, determines how near this function is to pure exponential decay, which would have $c = 0$ (in which case Eq. (B-1) would not apply). For the fits to polyethylene-protected Walls 2, 4, and 7, which could only dry outward, the best fit $c$ value was 1.33, whereas for the other kraft-faced walls, $c = 0.373$. To illustrate the effects of both $c$ and $\tau$, the function is plotted in Figure 47 with $\tau$ values that correspond to minimum, average, and maximum values of time constant (days) for the polyethylene walls with $c = 1.33$, along with a comparison at $\tau = 5$ for the kraft wall $c$ value of 0.373. We applied a scale factor of 12 to the function here, which made the numbers look similar to our OSB values of $M5_{net}$.

Inspection of Figure 47 confirmed that small values of $\tau$ indicated more rapid drying. In the actual fits to individual walls, the scale factor was allowed to vary to best match the overall $M5_{net}$ values for that wall but was required to be within ±0.9% MC of the starting value. Starting values were determined by picking the highest daily $M5_{net}$ recorded for the wall after the injection and resetting time zero to correspond to that peak value for each wall. Optimization of the fit parameters was done in Excel (Microsoft, Redmond, Washington, USA) by minimizing the sum of the squared errors (difference between function prediction and measured $M5_{net}$ value for each day after peak). Across all walls, the scale factors varied between 8 and 18.5 with average near 12, whereas $\tau$ values ranged from 3.8 to 103 with average of 17 for kraft walls and 27 for polyethylene walls. All kraft walls were required to share the same $c$ value. Similarly, all polyethylene walls shared a $c$ value, but it was higher, reflecting the slower outward-only drying of these walls. For Figure 42, which compares $\tau$ values across all wall types, the fit was changed to force a consistent $c$ value ($c = 0.76$), allowing direct comparison of $\tau$ values. Two examples of these fits are provided in Figure 48.

Using Excel in this manner does not provide any estimates of the uncertainty in fit parameters. Much of the error in this quantification method is a result of the bias of the model. An underlying assumption in the decay model is that all walls are driven to return to $M5_{net}$ zero after application of the water injection. Clearly, this assumption was not usually valid because the walls were subjected to

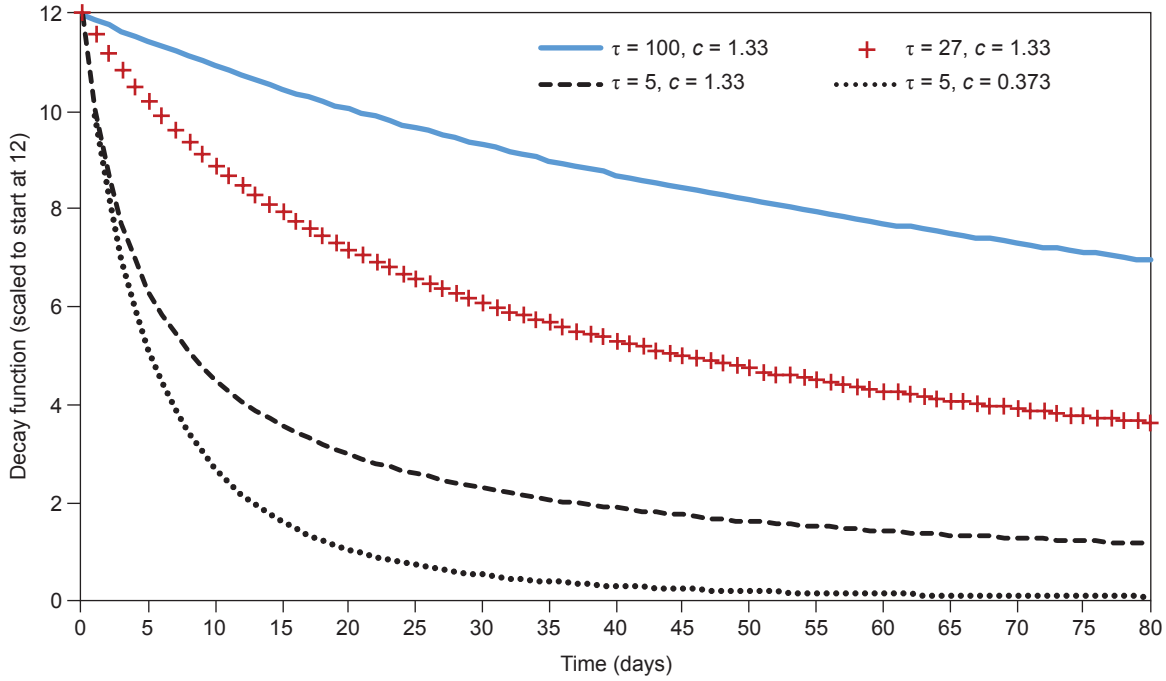


**Figure 47. Near-exponential decay function with $c = 1.33$, various $\tau$, and one value at $c = 0.373$ (similar to pure exponential decay).**

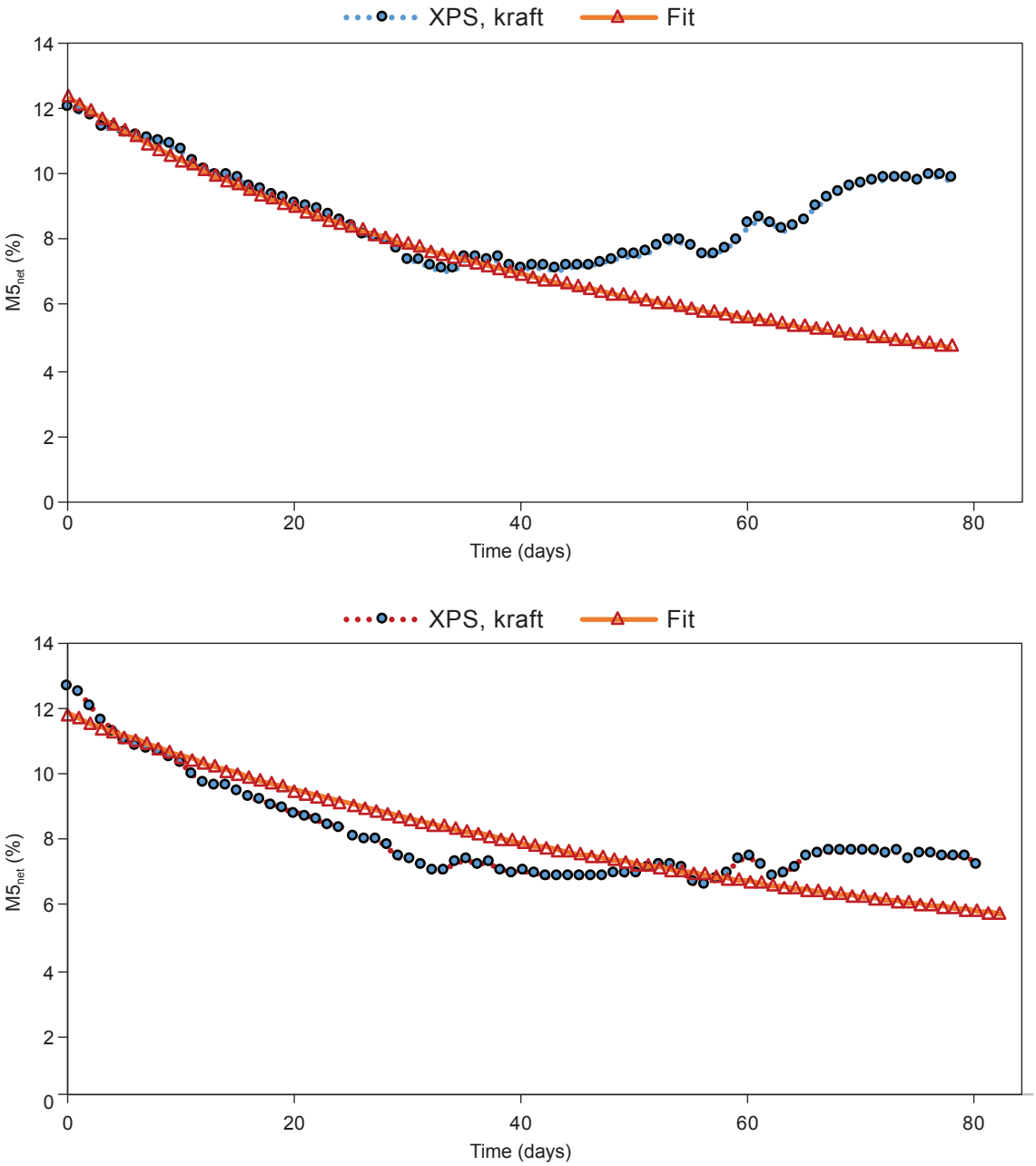


**Figure 48. $M5_{net}$ values after Injection 2 (Nov. 2015) in select north walls showing data and curve fit (XPS, extruded polystyrene).**

a variety of different driving forces with time. However, the experimental observation that many walls returned to near zero before Injection 3 provides some support for this bias in the model. Another bias is the assumption of uniform decay which reflects a single physical mechanism decreasing the MC at MC5. Clearly, this assumption is also not usually valid since water is moving away from MC5 because of leaving the system (escape to indoor or outdoor) and redistribution within the OSB. We have no data to show the magnitude of these two mechanisms, but we assume that most of the redistribution happens early; therefore, fitting the later data is able to capture much of the actual drying.

Further difficulty in quantifying the error of these decay constants, $\tau$, resulted from the variance within the data. Some of this variance did not reflect actual changes in MC of the OSB but was the result of electrical connection faults between the wires and the moisture pins, which resulted in data that jumped between infinite resistance (MC near 8%) and the actual value, as can be seen in some of the data

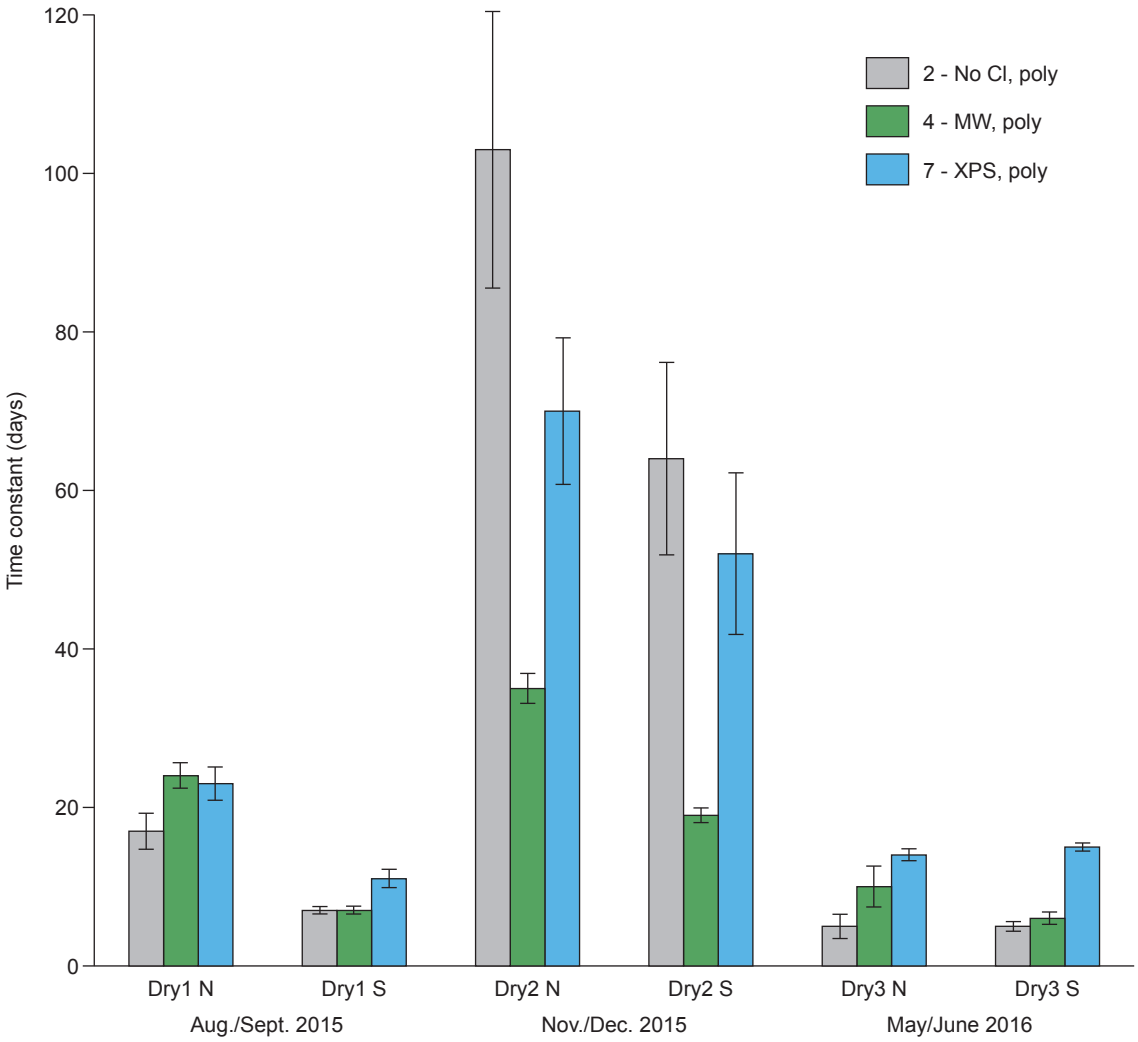


**Figure 49. Drying time constants for walls with polyethylene indoor barrier, including error bars from data variance but not model bias (CI, continuous insulation; MW, mineral wool; XPS, extruded polystyrene).**

sets (see Figures 32 and 33, for example). Given all these difficulties, the τ values should be used only to compare walls experiencing similar conditions, hence the grouping of the polyethylene walls in Table 4 and the kraft walls in Table 5.

Finally, to give an indication of the variance within the existing data and its effect on the fit parameters given the mentioned constraints, error bars are provided (excluding all the model bias) by fitting the polyethylene data sets using MATLAB, which provides estimates of the error in τ for the 95% confidence interval. These error bars are displayed in Figure 49.

## References

Baechler, M.C. [and others]. 2010. Guide to determining climate regions by county. PNNL-17211. Building America Best Practice Series Volume 7.1. Contract DE-AC05-76RLO 1830. Washington, DC: U.S. Department of Energy.

Boardman, C.R.; Glass, S.V.; Lebow, P.K. 2017. Simple and accurate temperature correction for moisture pin calibrations in oriented strand board. Building and Environment. 112: 250-260.

Buck, A.L. 1981. New equations for computing vapor pressure and enhancement factor. Journal of Applied Meteorology and Climatology. 20: 1527-1532.

Carll, C.G.; Boardman, C.R.; Verrill S.P. 2013. Durability of hardboard lap siding: performance in laboratory testing and in long-term exterior exposure. Res. Pap. FPL-RP-674.

Madison, WI: U.S. Department of Agriculture, Forest Service, Forest Products Laboratory. 25 p.

Carll, C.G.; Highley, T.L. 1999. Decay of wood and wood-based products above ground in buildings. Journal of Testing and Evaluation. 27(2): 150-158.

Craven, C.M.; Garber-Slaght, R.L. 2012. Exterior insulation envelope retrofits in sub-arctic environments. In: Proceedings, Seventh International Cold Climate HVAC Conference. Calgary, Alberta, Canada. Nov. 12-14, 2012: 1-8.

Craven, C.M.; Garber-Slaght, R.L. 2014. Exterior insulation envelope retrofits in cold climates: implications for moisture control. HVAC&R Research. 20: 384-394.

Duff, J.E. 1968. Moisture content distribution in wood-frame walls in winter. Forest Products Journal. 18(1): 60-64.

Fox, M.; Straube, J.; Ge, H.; Trainor, T. 2014. Field test of hygrothermal performance of highly insulated wall assemblies. In: Proceedings, 14th Canadian Conference on Building Science and Technology. Toronto, Ontario, Canada. Oct. 28-30, 2014: 101-110.

Glass, S.V.; TenWolde, A. 2007. Review of in-service moisture and temperature conditions in wood-frame buildings. Gen. Tech. Rep. FPL-GTR-174. Madison, WI: U.S. Department of Agriculture, Forest Service, Forest Products Laboratory. 53 p.

Glass, S.V.; Zelinka, S.L.; Johnson, J.A. 2014. Investigation of historic equilibrium moisture content data from the Forest Products Laboratory. Gen. Tech. Rep. FPL-GTR-229. Madison, WI: U.S. Department of Agriculture, Forest Service, Forest Products Laboratory. 34 p.

ICC. 2015. International Energy Conservation Code. Country Club Hills, IL: International Code Council.

Kane, R.; Titley, G. 1987. Case histories of moisture monitoring in residential walls. In: Powell, F.J.; Matthews, S.L., eds. Thermal insulation: materials and systems, ASTM Special Technical Publication 922. Philadelphia, PA: American Society for Testing and Materials: 615-629.

Lstiburek, J.W. 2004. Understanding vapor barriers. ASHRAE Journal. 46(8): 40-50.

Lstiburek, J.W. 2013a. Joni Mitchell, water & walls. ASHRAE Journal. 55(8): 72-80.

Lstiburek, J.W. 2013b. ‘Double, double toil and trouble’: Macbeth does vapor barriers. ASHRAE Journal. 55(11): 56-62.

Lstiburek, J.W. 2016. Doubling down: How come double vapor barriers work? ASHRAE Journal. 58(1): 52-59.

Maref, W.; Rousseau, M.Z.; Armstrong, M.M.; Lee, W.; Leroux, M.; Nicholls, M. 2011. Evaluating the effects of two energy retrofit strategies for housing on the wetting and drying potential of wall assemblies: summary report for year 2007-08 phase of the study. RR-315. Ottawa, Canada: National Research Council Canada.

Parsons, G.D.; Lieburn, B.; Stewart, G.; Eastman, P. 2016. Comparison of measured hygrothermal performance of wood-frame walls built with continuous exterior insulation versus walls built with housewrap and oriented strand board sheathing in single-family homes in a cold climate. In: Proceedings, Thermal Performance of the Exterior Envelopes of Whole Buildings XIII, Clearwater, FL. Atlanta, GA: American Society of Heating, Refrigerating and Air-Conditioning Engineers.

Proskiw, G. 1995. The performance of energy-efficient residential building envelope systems. In: Proceedings, Thermal Performance of the Exterior Envelopes of Buildings VI, Clearwater, FL. Atlanta, GA: American Society of Heating, Refrigerating and Air-Conditioning Engineers: 391-398.

Rose, W.B.; McCaa, D.J. 1998. Temperature and moisture performance of wall assemblies with fiberglass and cellulose insulation. In: Proceedings, Thermal Performance of the Exterior Envelopes of Buildings VII, Clearwater, FL. Atlanta, GA: American Society of Heating, Refrigerating and Air-Conditioning Engineers: 133-144.

Sherwood, G.E. 1983. Condensation potential in high thermal performance walls – cold winter climate. Res. Pap. FPL 433. Madison, WI: U.S. Department of Agriculture, Forest Service, Forest Products Laboratory.

Smegal, J.; Grin, A. 2015. Inward vapor drives in adhered veneer wall assemblies with continuous exterior insulation. In: Proceedings, Fourth Conference on Building Enclosure Science & Technology (BEST 4). Kansas City, MO, Apr. 13-15, 2015.

Smegal, J.; Straube, J.; Lstiburek, J.; Grin, A. 2013. Moisture-related durability of walls with exterior insulation in the Pacific Northwest. In: Proceedings, Thermal Performance of the Exterior Envelopes of Whole Buildings XII International Conference. Clearwater, FL. Dec. 1-5, 2013. Atlanta, GA: American Society of Heating, Refrigerating and Air-Conditioning Engineers.

Straube, J. 2011. Controlling cold-weather condensation using insulation. Building Science Digest 163. Somerville, MA: Building Science Press.

Straube, J.F.; Burnett, E.F.P. 1998. Drainage, ventilation drying, and enclosure performance. In: Proceedings, thermal performance of the exterior envelopes of buildings VII. Atlanta: American Society of Heating, Refrigerating and Air-Conditioning Engineers: 189-198.

TenWolde, A.; Carll, C.; Malinauskas, V. 1995. Airflows and moisture conditions in walls of manufactured homes. In: Modera, M.P.; Persily, A.K., eds. Airflow performance

of building envelopes, components, and systems. ASTM STP 1255. Philadelphia: American Society for Testing and Materials: 137-155.

TenWolde, A.; Rose, W.B. 1996. Moisture control strategies for the building envelope. Journal of Thermal Insulation and Building Envelopes. 19: 206-214.

Trainor, T.; Smegal, J. 2017. Analysis of exterior insulated high-R wall systems. Ottawa, Ontario, Canada: Natural Resources Canada.

Trainor, T.M.; Smegal, J.; Straube, J.; Parekh, A. 2016. Measured and predicted moisture performance of high-R wall assemblies in cold climates. In: Proceedings, Thermal Performance of the Exterior Envelopes of Whole Buildings XIII, Clearwater, FL. Atlanta, GA: American Society of Heating, Refrigerating and Air-Conditioning Engineers.

Tsongas, G.A. 1991. The effect of exterior insulating sheathing on wall moisture. In: Graves, R.S.; Wysocki, D.C., eds. Insulation materials: testing and applications, 2nd Volume. Philadelphia: American Society for Testing and Materials: 401-414.

Van Straaten, R. 2003. Measurement of ventilation drying of vinyl siding and brick clad wall assemblies. Waterloo, Ontario, Canada: University of Waterloo, Department of Civil Engineering. M.S. thesis.

Wang, F.S. 1981. Comparative studies of vapor condensation potentials in wood framed walls. In: Proceedings of the ASHRAE/DOE–ORNL Conference, Thermal Performance of the Exterior Envelopes of Buildings. ASHRAE SP 28. New York: American Society of Heating, Refrigerating and Air-Conditioning Engineers: 836-846.

Whitehead, L.; Whitehead, R.; Valeur, B.; Berberan-Santos, M. 2009. A simple function for the description of near-exponential decays: The stretched or compressed hyperbola. American Journal of Physics. 77: 173. (http://dx.doi.org/10.1119/1.3008007).

Wilkinson, J.; Ueno, K.; De Rose, D.; Straube, J.F.; Fugler, D. 2007. Understanding vapour permeance and condensation in wall assemblies. In: Proceedings, 11th Canadian Conference on Building Science and Technology, Banff, Alberta, Canada. March 22-23, 2007. Vancouver, British Columbia, Canada: British Columbia Building Envelope Council.